Surface electronic structure

1982 Rep. Prog. Phys. 45 223

(http://iopscience.iop.org/0034-4885/45/3/001)

Rep. Prog. Phys., Vol. 45, 1982. Printed in Great Britain

Surface electronic structure

J E Inglesfield

Science and Engineering Research Council, Daresbury Laboratory, Daresbury, Warrington WA4 4AD, UK

Abstract

The theory of the electronic structure of clean metal and semiconductor surfaces is reviewed, starting from an effective one-electron Schrödinger equation. Methods for solving the Schrödinger equation at surfaces are briefly described, and the effects of the surface on the electronic wavefunctions are discussed using simple models. The results of detailed calculations of the surface electronic structure of s–p bonded metals, transition metals and semiconductors are reviewed, with an emphasis on the effect of the local environment on the density of states. Properties like the work function and surface energy depend on the surface electronic structure, and their variation with material and surface is discussed; the surface energy contains an important contribution from the interaction between electrons, and this will be considered in some detail. The change in electronic structure compared with the bulk leads to changes in atomic structure, with surface reconstruction on semiconductor and some metal surfaces, and this is also discussed. The interplay between theory and experiment is very important in surface studies, and the theoretical surface energy bands reviewed in this article compare well with experimental photoemission results; this comparison has proved particularly useful for understanding surface reconstructions.

This review was received in August 1981.

0034–4885/82/030223+62$08.00

Contents

1. Introduction

As anyone who has suffered from a rusting car knows, surface processes play a significant part in our lives—corrosion on the car body, friction in the wear and tear on the engine, catalysis in the petrol refining, all occur at surfaces. These processes all depend on the interplay between the electronic structure and atomic structure of imperfect, dirty surfaces in complicated ways. Before we can tackle these we must first understand clean, perfect surfaces, and in recent years there has been great progress on both the theoretical and experimental fronts. Self-consistent calculations have been made for the electronic structure of many surfaces, giving the charge density, density of electronic states (e.g. Krakauer *et al* 1979a) and in some cases the surface energy (Appelbaum and Hamann 1978): from the charge density, the work function can be found—the energy needed to remove an electron from the solid, which is very important in devices like image intensifiers; the surface energy is itself important in understanding adhesion and wetting. The stable atomic structure depends on the electronic structure, and here calculations have shown why some semiconductors (Chadi 1978) and metal surfaces (Inglesfield 1981) reconstruct, with the atoms moving from the positions they would have in the bulk.

The surface electronic structure can be probed experimentally using angle-resolved photoemission in which the energy distribution of photoemitted electrons is studied at different angles (Feuerbacher *et al* 1978); encouraging agreement has given confidence in calculations of the surface electronic structure (Ihm *et al* 1980). Features in the photoemission spectra can come from electronic transitions in the bulk of the solid (Dietz and Eastman 1978) as well as transitions involving electronic states at the surface, but there are experimental methods for separating out the surface features (Plummer and Eberhardt 1979)—their insensitivity to photon frequency (bulk transitions can only take place if $\hbar\omega$ equals the energy between occupied and unoccupied states with the same Bloch wavevector) and the sensitivity to adsorption of H, for example (Campuzano *et al* 1980). But the most definitive interpretations of photoemission spectra have come from comparison with photoemission calculations which themselves involve calculations of the surface electronic structure (Pendry and Hopkinson 1978a). The interdependence of the surface electronic and atomic structure means that the comparison between photoemission spectra and calculations can sometimes be used to distinguish between possible surface geometries. This is particularly useful for a reconstructed surface with a large surface unit mesh, such as the (7×7) reconstruction† of Si (111) (Chadi *et al* 1980), or when there is no long-range order (Chabal *et al* 1981). In such cases the usual method of determining the surface atomic structure, analysis of low-energy electron diffraction (LEED) data (Pendry 1974), may be impractical. The electrostatic potential at the surface can be probed using x-ray photoemission, in which an electron is emitted from an atomic core level, whose energy depends on the local potential: this is useful for studying charge transfer at the surface (Brennan *et al* 1980). Photoemission is certainly the most powerful

† A (1×1) surface has the unit mesh obtained by continuing the bulk structure to the surface, with lattice vectors $\boldsymbol{a}, \boldsymbol{b}$. A $(m\times n)$ surface has a unit mesh with lattice vectors $m\boldsymbol{a}, n\boldsymbol{b}$.

experimental probe, but field emission has also been useful (Plummer and Gadzuk 1970), in which an applied electric field pulls electrons very close to the Fermi level out of the solid.

An atom at the surface is in an environment midway between the bulk and the isolated atom, and this is reflected in the 'local density of states', which is the charge density of electrons at a particular energy. The local density of states at a surface is made up of the tails of bulk wavefunctions, as well as an extra type of solution of the Schrödinger equation—surface states—which are wavefunctions localised at the surface (Forstmann 1978). Surface states are greatly influenced by the surface atomic structure, and play an important role in the reconstruction of semiconductors (Appelbaum and Hamann 1975) (but probably not metals). Surface states occur both on semiconductor and metal surfaces, but on semiconductors they sometimes have the character of dangling bonds (Appelbaum and Hamann 1973)—chemical bonds which are cut when the surface is made. The interpretation of the electronic structure in terms of local chemical bonds works quite well on semiconductor and insulator surfaces, but is not so useful for metals whose valence orbitals are less directional, and whose bonding is not covalent. As in the bulk metals, where the free-electron model is useful, the surface of jellium, in which the atomic potentials are smeared out into a uniform positive background, provides a useful starting point for understanding the surface electronic structure of metals like Na and Al (Lang 1973). In the transition metals where the d electrons dominate the bonding, the tight-binding (LCAO) method provides a useful starting point (Friedel 1973). The change in the local density of states at the surface of transition metals can, in fact, lead to changes in magnetism, with the possibility of reduced magnetism at the surface of ferromagnets (Liebermann *et al* 1970) or ferromagnetism at the surface of paramagnets (Akoh and Tasaki 1978).

The calculation of surface electronic structure is made possible because it is a good approximation to treat the interaction between electrons within a one-electron formalism: each electron moves in an effective potential due to the smeared-out charge density of all the other electrons (Kohn and Sham 1965). This approach can be fully justified as far as the calculation of the ground-state properties like charge density and energy are concerned (Hohenberg and Kohn 1964)—at least, we know that the effective potential exists and the approximation comes in finding it. The one-electron approach also works remarkably well in calculating the electronic excitations probed in photoemission experiments (Dietz and Eastman 1978). However, there are some genuine many-body effects at surfaces, with the possibility of collective electron oscillations localised at the surface, the surface plasmons, which can be excited in electron energy-loss experiments (Krane and Raether 1976). The surface plasmons are responsible for the image interaction of an external charge with a surface (Ritchie 1972) and for the van der Waals' interaction (Inglesfield and Wikborg 1975). But as far as surface bonding and electronic structure are concerned—the subject of this review—we can neglect many-body effects explicitly and work with an effective single-particle Schrödinger equation. This is by no means trivial to solve as the potential felt by an electron does not have the full three-dimensional symmetry of the bulk crystal, and the effective potential due to the other electrons must be determined self-consistently, by iteration. It is the complexity and scale of this computing task which held up really reliable surface calculations until comparatively recently, and even now plenty remains to be done.

1.1. Units

Atomic units are used, with $e = \hbar = m = 1$. The unit of energy is the Hartree (4.359×10^{-18} J), though sometimes we shall use eV (27.2 eV = 1 au); the unit of length is the Bohr radius (5.292×10^{-11} m). The electron density is usually given in terms of r_s, the radius of a sphere containing one electron.

2. Electronic states at the surface

2.1. The Schrödinger equation at the surface

The problem of calculating the electronic structure of a solid with a surface is fairly formidable, as there are 10^{23} electrons all interacting with one another, and with the ions. We can make progress, however, by replacing the full many-body Schrödinger equation by an effective one-particle equation (Kohn and Sham 1965, Lang 1973):

$$-\tfrac{1}{2}\nabla^2\psi_i(\boldsymbol{r}) + \Big(\sum_{\mathrm{I}} v_{\mathrm{ion}}(\boldsymbol{r}-\boldsymbol{r}_{\mathrm{I}}) + V_{\mathrm{H}}(\boldsymbol{r}) + V_{\mathrm{xc}}(\boldsymbol{r})\Big)\psi_i(\boldsymbol{r}) = \epsilon_i\psi_i(\boldsymbol{r}) \tag{2.1}$$

in which the electron feels the potential due to the ions v_{ion}, the Hartree potential $V_{\mathrm{H}}(\boldsymbol{r})$, the electrostatic potential due to the smeared-out charge density of all the other electrons, and the exchange-correlation potential $V_{\mathrm{xc}}(\boldsymbol{r})$ to allow for the fact that the electrons actually move in a correlated way. The ground-state charge density is given by a sum over occupied states (each containing two electrons):

$$\rho_0(\boldsymbol{r}) = 2\sum_{\substack{\text{occupied}\\ i}} |\psi_i(\boldsymbol{r})|^2 \tag{2.2}$$

and the ground-state energy by

$$E_0 = 2\sum_{\substack{\text{occupied}\\ i}} \epsilon_i - \tfrac{1}{2}\int \mathrm{d}\boldsymbol{r}\, V_{\mathrm{H}}(\boldsymbol{r})\rho_0(\boldsymbol{r}) - \int \mathrm{d}\boldsymbol{r}\, V_{\mathrm{xc}}(\boldsymbol{r})\rho_0(\boldsymbol{r}) + E_{\mathrm{xc}} \tag{2.3}$$

the sum of one-electron energy levels, with the electrostatic Hartree interaction subtracted to avoid double counting and the exchange-correlation energy E_{xc} explicitly added. The charge density and effective potentials must be determined self-consistently, the Hartree potential being given by

$$V_{\mathrm{H}}(\boldsymbol{r}) = \int \mathrm{d}\boldsymbol{r}'\, v(\boldsymbol{r}-\boldsymbol{r}')\rho_0(\boldsymbol{r}'). \tag{2.4}$$

The exchange-correlation potential depends on all the details of the charge density, and formally it is the functional derivative of E_{xc} with respect to ρ_0:

$$V_{\mathrm{xc}}(\boldsymbol{r}) = \frac{\delta E_{\mathrm{xc}}[\rho_o(\boldsymbol{r})]}{\delta\rho_o(\boldsymbol{r})}. \tag{2.5}$$

Of course we do not know this functional dependence in general, but it is a good approximation to make the local density approximation (Hohenberg and Kohn 1964, Kohn and Sham 1965, Lang 1973), in which E_{xc} is written:

$$E_{\mathrm{xc}} \approx \int \mathrm{d}\boldsymbol{r}\, \rho_0(\boldsymbol{r})\epsilon_{\mathrm{xc}}(\rho_0) \tag{2.6}$$

where $\epsilon_{xc}(\rho_0)$ is the exchange-correlation energy per electron of an infinite homogeneous electron gas with the local density ρ_0; V_{xc} then becomes

$$V_{xc}(\boldsymbol{r}) = \frac{d}{d\rho}\{\rho\epsilon_{xc}(\rho)\}\Big|_{\rho=\rho_0}. \tag{2.7}$$

Generalisations of the RPA (von Barth and Hedin 1972) or an interpolation scheme between the high- and low-density limits (Lang 1973) are usually used to find ϵ_{xc}.

The effective single-particle approach (2.1)–(2.3) can be rigorously justified for the ground-state energy and charge density using density functional theory (Hohenberg and Kohn 1964); the method is so useful because the local density approximation for E_{xc} and V_{xc} (2.6)–(2.7) works well, even when the electron density varies rapidly as in molecules (Gunnarsson *et al* 1977) and at a surface (Lang and Sham 1975, Langreth and Perdew 1977). Moreover it can be generalised to magnetic materials (Wang and Callaway 1977) using the spin-polarised local density approximation, in which electrons with different spin are allowed to have a different density and feel a different exchange-correlation potential (von Barth and Hedin 1972). The application to bulk band structure calculations has been summarised in a recent review article by Koelling (1981). In principle, the energy eigenvalues ϵ_i and wavefunctions ψ_i in (2.1) have no individual meaning in density functional theory (Lang 1973)—it is only the ground-state quantities constructed from them like ρ_0 and E_0 which we can rely on. Nevertheless in practice these energies correspond quite closely to the one-electron excitation energies (Dietz and Eastman 1974, Pendry and Hopkinson 1978b, Thiry *et al* 1979, Eastman *et al* 1980): the change in energy when an electron is added or removed from the system—in other words, the energy levels which are measured in experiments like photoemission. The excitation energies and quasiparticle wavefunctions can, in fact, be calculated rigorously from a single-particle Schrödinger equation containing an energy-dependent non-local self-energy (Hedin and Lundqvist 1969); this is very difficult to calculate except in simple models, but these can be used to find the corrections to the excitation energies from (2.1) (Treglia *et al* 1980).

Having simplified the many-body problem we are left with a total effective potential $V(\boldsymbol{r})$, due to the positive ions, Hartree and exchange-correlation potentials, of the form shown in figure 1—as an electron approaches the solid from vacuum it feels the image potential, and then a crystal potential which reaches the bulk value within an atomic spacing or so from the surface. The image potential, which actually becomes the exchange-correlation potential when the electron enters the solid, has the asymptotic form:

$$V(z) \sim -1/4|z| \tag{2.8}$$

in the case of metals; there is an extra factor of $\frac{1}{2}$ compared with the electrostatic potential because the image potential is a polarisation energy. The local density approximation does not give the asymptotic form of $V(z)$ correctly, but rather gives an exchange-correlation potential decreasing exponentially into the vacuum, as a result of the exponential decay of the tail of the electronic charge distribution. In fact, it makes little difference to use the exponential form rather than (2.8) in calculations of the ground-state properties (Lang and Kohn 1970), because there is so little electronic charge in the region where the asymptotic behaviour prevails (though it is important to use (2.8) in calculations of positrons at metal surfaces, as positrons may be repelled from the bulk and sit trapped in the $-1/4|z|$ image potential (Pendry 1980a)). The potential in the actual surface region, i.e. the top layer or two of atoms,

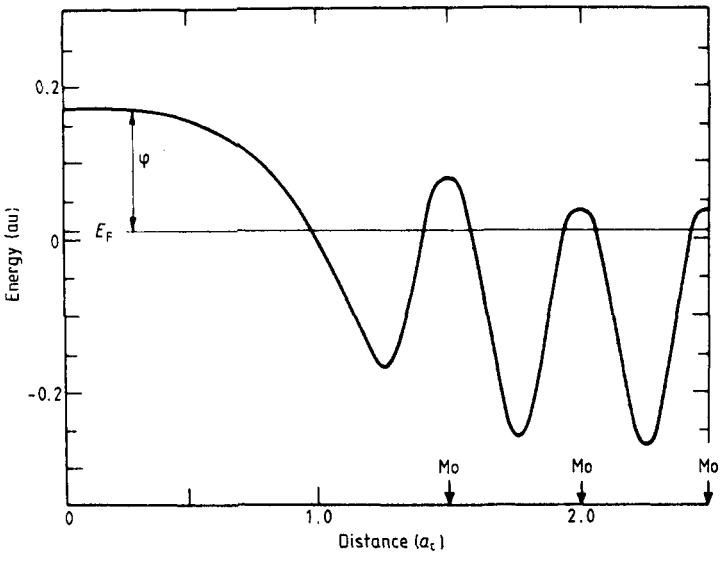

Figure 1. Potential at Mo (001) surface (averaged parallel to the surface). Arrows mark the positions of atomic layers and φ is the work function (Kerker *et al* 1978).

depends crucially on the self-consistently determined charge density. The charge redistribution at the surface sets up a surface barrier which determines the absolute value of the bulk potential with respect to vacuum, hence the work function φ (figure 1), and measurement of φ provides a good check on the accuracy of self-consistent calculations (§ 5). As V goes rapidly to the bulk value it is adequate for some purposes (in calculations of LEED (Pendry 1974) and photoemission from close-packed metal surfaces, for example) to approximate the surface barrier by a step potential, using the bulk potential right up to the geometrical surface.

2.2. Wavefunctions at the surface

The two-dimensional periodicity of the potential at the surface of a perfect crystal means that the wavefunctions can be characterised by a two-dimensional Bloch wavevector $\boldsymbol{K}$ (Pendry 1974) such that

$$\psi_{\boldsymbol{K}}(\boldsymbol{R}+\boldsymbol{R}_{\mathrm{I}}, z) = \exp(\mathrm{i}\boldsymbol{K}\cdot\boldsymbol{R}_{\mathrm{I}})\psi_{\boldsymbol{K}}(\boldsymbol{R}, z) \tag{2.9}$$

a displacement through a surface lattice vector $\boldsymbol{R}_{\mathrm{I}}$ multiplies the wavefunction by $\exp(\mathrm{i}\boldsymbol{K}\cdot\boldsymbol{R}_{\mathrm{I}})$. (We choose coordinates so that z is perpendicular to the surface, and $\boldsymbol{R}=(x, y)$ lies in the surface.) $\boldsymbol{K}$ does not label ψ uniquely, and at each wavevector there are bands of continuum states coming from the bulk energy bands and possibly discrete states—the surface states—localised at the surface; $\boldsymbol{K}$ itself is not given uniquely, but a surface reciprocal lattice vector $\boldsymbol{G}$ may be added to it. When an electron leaves a solid surface in the photoemission process, going into a plane wave in the vacuum, $\boldsymbol{K}$ is conserved (to within $\boldsymbol{G}$), and this makes angle-resolved photoemission such a powerful tool for studying electron states at the surface. A good example of umklapp by $\boldsymbol{G}$ comes from angle-resolved photoemission experiments on the W (001) surface: when the W (001) surface is cooled below room temperature

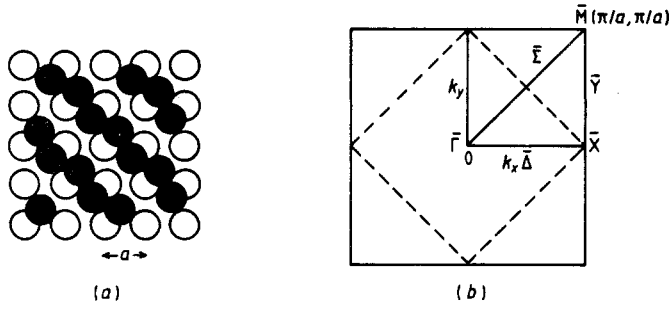

Figure 2. (*a*) W (001) $(\sqrt{2}\times\sqrt{2})$ R45° surface reconstruction; shaded circles show surface atoms and open circles the layer beneath. (*b*) First Brillouin zone of (1×1) structure (full line) and $(\sqrt{2}\times\sqrt{2})$ R45° structure (broken line).

the (1×1) structure reconstructs to form a $(\sqrt{2}\times\sqrt{2})$ R45° structure† (Debe and King 1979) (figure 2); extra features then develop in angle-resolved photoemission at $\boldsymbol{K}=(\pi/a, \pi/a)$ corresponding to features in emission normal to the surface ($\boldsymbol{K}=0$) (Campuzano *et al* 1981) (figure 3), due to electrons with $\boldsymbol{K}=0$ being scattered through a new surface reciprocal lattice vector $\boldsymbol{G}=(\pi/a, \pi/a)$.

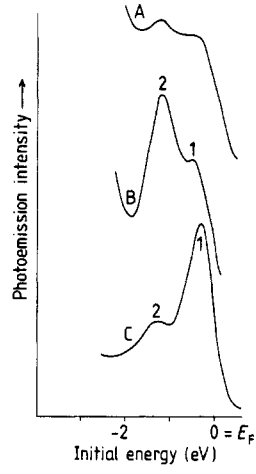

Figure 3. Photoemission energy distribution for electrons emitted with $\boldsymbol{K}\approx(\pi/a, \pi/a)$ from W (001) (1×1) (curve A) and $(\sqrt{2}\times\sqrt{2})$ R45° structure (curve B). Features 1 and 2 occur at same energies as features in normal emission (curve C) (Campuzano *et al* 1981).

The Bloch property of $\psi_{\boldsymbol{K}}$ means that it is only necessary to solve the Schrödinger equation in one surface unit cell, but we must still integrate the equation in the z direction—fortunately, the wavefunctions away from the surface can be written in terms of solutions of the bulk Schrödinger equation (Heine 1963). The simplest case to consider is the step potential model of a free-electron solid surface, with a constant potential of $-V_0$ inside the solid ($z>0$) and zero in vacuum ($z<0$), actually quite a realistic model of s–p bonded metals like Al in which the pseudopotential is weak. The bulk free-electron wave

$$\varphi_{\boldsymbol{K},-k_z}(\boldsymbol{r})=\exp\left[\mathrm{i}(\boldsymbol{K}\cdot\boldsymbol{R}-k_z z)\right] \tag{2.10}$$

† A $(\sqrt{2}\times\sqrt{2})$ R45° surface has lattice vectors which are $\sqrt{2}\times$ the original lattice vectors in length, rotated by 45°.

is reflected by the surface into $\exp[i(\boldsymbol{K}\cdot\boldsymbol{R}+k_z z)]$, and the full solution of the Schrödinger equation at energy E with wavevector $\boldsymbol{K}$ can be written:

$$\psi_{\boldsymbol{K},E}(\boldsymbol{r})=\varphi_{\boldsymbol{K},-k_z}(\boldsymbol{r})+a\varphi_{\boldsymbol{K},+k_z}(\boldsymbol{r}) \qquad z>0, \text{ in solid} \tag{2.11}$$

$$\psi_{\boldsymbol{K},E}(\boldsymbol{r})=b\exp(i\boldsymbol{K}\cdot\boldsymbol{R})\exp(\gamma' z) \qquad z<0, \text{ in vacuum} \tag{2.12}$$

$$k_z=(2E-K^2)^{1/2} \qquad \gamma'=[K^2+2(V_0-E)]^{1/2}. \tag{2.13}$$

E is measured from the bulk potential. The coefficients a and b are determined by the condition that the amplitude and derivative of ψ are continuous across the surface at $z=0$.

When the full crystal potential is included, the surface can scatter the incident wave by a surface reciprocal lattice vector, and it is necessary to generalise (2.11) (Heine 1963). The bulk wavefunctions are usually labelled by the reduced three-dimensional Bloch wavevector $\boldsymbol{k}$ and a band index, but for our purposes it is convenient to relabel them: the states with reduced wavevector component $\boldsymbol{K}$ parallel to the surface and energy E, travelling in the + or − z direction, can be identified uniquely by a surface reciprocal lattice vector $\boldsymbol{G}$. In a nearly-free-electron crystal the energies of wavefunctions with reduced three-dimensional wavevector $\boldsymbol{k}$ are given by

$$E=\tfrac{1}{2}[(k_x+g_x)^2+(k_y+g_y)^2+(k_z+g_z)^2] \tag{2.14}$$

where $\boldsymbol{g}=(g_x, g_y, g_z)$ is a bulk reciprocal lattice vector. The projection of $\boldsymbol{g}$ onto the surface plane, $\boldsymbol{G}=(g_x, g_y)$, is a surface reciprocal lattice vector (Inglesfield 1978a), so for a given $\boldsymbol{K}$, $\boldsymbol{G}$ and E, $+(k_z+g_z)$ is determined uniquely; as the shortest bulk reciprocal lattice vector perpendicular to the surface equals $2\pi/d$, where d is the interlayer spacing, this corresponds to a unique value of k_z in the range $-\pi/d$ to $+\pi/d$. We can then identify the bulk wavefunctions by $\varphi^{\pm}_{\boldsymbol{K},\boldsymbol{G};E}$, where $\boldsymbol{K}$ lies in the surface Brillouin zone and + or − identifies the wave as travelling in the positive or negative z direction. This labelling still holds when the crystal potential is switched on (Heine 1963). We can now consider a bulk wave $\varphi^{-}_{\boldsymbol{K},\boldsymbol{G};E}$ travelling towards the surface—this is reflected and scattered by the surface, and the total wavefunction is given by the generalisation of (2.11) (Heine 1963, Appelbaum and Hamann 1972, Pendry 1974):

$$\psi_{\boldsymbol{K},\boldsymbol{G};E}(\boldsymbol{r})=\varphi^{-}_{\boldsymbol{K},\boldsymbol{G};E}(\boldsymbol{r})+\sum_{\boldsymbol{G}'} a_{\boldsymbol{G},\boldsymbol{G}'}\varphi^{+}_{\boldsymbol{K},\boldsymbol{G}';E}(\boldsymbol{r}) \qquad z>0 \tag{2.15}$$

with coefficients determined by matching the wavefunction and its derivative onto the vacuum wavefunction, or more accurately the vacuum wavefunction integrated through the surface barrier region. The sum over reflected waves actually includes waves decaying exponentially away from the surface, as well as true bulk wavefunctions travelling away from the surface: these correspond to energies lying in a bulk band gap, or large values of $\boldsymbol{G}$ in (2.14), when k_z is complex—such waves which increase or decrease exponentially are not allowed in an infinite crystal, but the solution decaying away from the surface is allowed in the semi-infinite crystal (Pendry 1974).

For every wavefunction in the bulk crystal travelling in the negative z direction, towards the surface, there is a wavefunction in the crystal with a surface of the form given by (2.15), and at fixed $\boldsymbol{K}$ there is a continuum of states as a function of energy, except in band gaps where there are no incident waves. The most useful function to consider in the continuum is the local density of states (Heine 1980), defined as

$$\sigma(\boldsymbol{r}, E)=\sum_i |\psi_i(\boldsymbol{r})|^2\,\delta(E-\epsilon_i) \tag{2.16}$$

the charge density of electrons with energy E. Sometimes it is convenient to restrict the sum over states i to states with a particular wavevector $\boldsymbol{K}$; we can integrate σ or $\sigma_{\boldsymbol{K}}$ through the surface atomic cell to give the surface density of states:

$$n_s(E) = \int_{\text{surface cell}} d\boldsymbol{r}\, \sigma(\boldsymbol{r}, E). \tag{2.17}$$

As an example, figure 4 shows the surface density of states for the Al (001) surface at $\boldsymbol{K} = (0.1, 0.1)$ au as a function of E, compared with the bulk density of states $n_{b,\boldsymbol{K}}$ with the same wavevector. We see that $n_{b,\boldsymbol{K}}$ has $|E-\epsilon_0|^{-1/2}$ singularities at the band edges, which become $|E-\epsilon_0|^{1/2}$ singularities in $n_{s,\boldsymbol{K}}$, completely general behaviour (Inglesfield 1978a). Except at the band edges $n_{s,\boldsymbol{K}}$ is rather close to $n_{b,\boldsymbol{K}}$, due to the Al atoms at the surface still having 8 of the 12 bulk nearest neighbours: unlike the individual wavefunctions which depend on distant boundary conditions, the local density of states really is a local property depending mainly on the atom and its environment (Heine 1980).

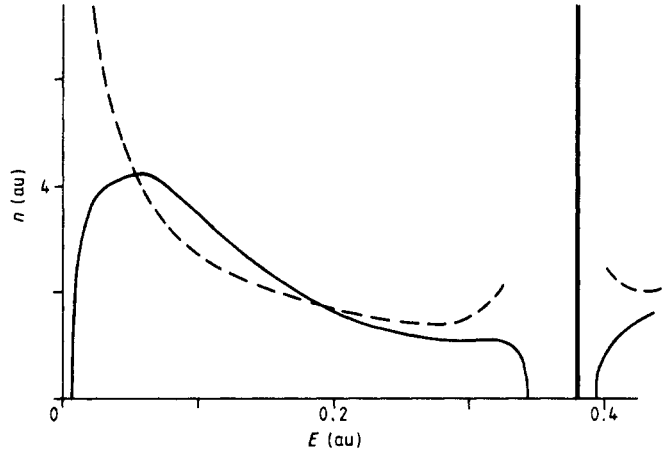

Figure 4. Surface density of states $n_{s,\boldsymbol{K}}(E)$ at $\boldsymbol{K} = (0.1, 0.1)$ au for Al (001) (full curve) compared with bulk density of states with the same wavevector $\boldsymbol{K}$ (broken curve).

The Al (001) surface density of states (figure 4) shows a discrete state in the bulk energy gap corresponding to a surface state, a wavefunction localised at the surface. In an absolute band gap there are no travelling waves with wavevector component $\boldsymbol{K}$, but it may be possible to construct a wavefunction from the forbidden bulk waves $\varphi^{\text{decay}}_{\boldsymbol{K},\boldsymbol{G};E}$ which decay exponentially away from the surface (Pendry and Gurman 1975):

$$\psi_{\boldsymbol{K},\boldsymbol{G};E}(\boldsymbol{r}) = \sum_{\boldsymbol{G}'} a_{\boldsymbol{G},\boldsymbol{G}'} \varphi^{\text{decay}}_{\boldsymbol{K},\boldsymbol{G}';E}(\boldsymbol{r}). \tag{2.18}$$

This crystal wavefunction and its normal derivative must be matched onto the vacuum wavefunction, and unlike in the continuum where the matching equations can always be solved, this is only possible at discrete energies; the resulting wavefunction decaying exponentially away from the surface in both directions is the surface state.

The simplest example of a surface state is in the band gap of a nearly-free-electron crystal with a one-dimensional potential varying like

$$V(z) = 2V_g \cos 2\pi z/a. \tag{2.19}$$

This potential opens up an energy gap in the band structure of the infinite crystal at $k_z = \pm\pi/a$, and around $k_z = \pi/a$ the solutions of the bulk Schrödinger equation can be written in the approximate form (Jones 1972):

$$\varphi_{\boldsymbol{K},k_z}(\boldsymbol{r}) = \exp(\mathrm{i}\boldsymbol{K}\cdot\boldsymbol{R})\{a\exp(\mathrm{i}k_z z) + b\exp[\mathrm{i}(k_z - g_z)z]\} \tag{2.20}$$

$$g_z = 2\pi/a.$$

Substituting this into the Schrödinger equation, and equating coefficients gives the matrix equation for a and b:

$$\begin{pmatrix} \frac{1}{2}(K^2+k_z^2)-E & V_g \\ V_g & \frac{1}{2}[K^2+(k_z-g_z)^2]-E \end{pmatrix}\begin{pmatrix} a \\ b \end{pmatrix} = 0 \tag{2.21}$$

which has a solution when

$$E = \tfrac{1}{2}K^2 + \tfrac{1}{4}([k_z^2+(k_z-g_z)^2] \pm \{[k_z^2-(k_z-g_z)^2]^2 + 16V_g^2\}^{1/2}). \tag{2.22}$$

If k_z is restricted to be real, as in the infinite crystal, this gives an energy gap of $2|V_g|$ at $k_z = \pi/a$. Energies in the gap correspond to complex $k_z = \kappa + \mathrm{i}\gamma$, and substituting into (2.22) we find

$$\kappa = \pi/a$$

$$\gamma = \pm\sqrt{2}\left(-\frac{\kappa^2}{2} - (E-\tfrac{1}{2}k^2) + [V_g^2 + 2(E-\tfrac{1}{2}k^2)\kappa^2]^{1/2}\right)^{1/2}. \tag{2.23}$$

γ starts off from zero at the bottom of the gap, increases to its maximum value of about $|V_g|(\pi/a)^{-1}$ close to the middle of the gap and decreases to zero at the top of the gap. The corresponding wavefunctions, forbidden in the bulk, have the form:

$$\varphi_{\boldsymbol{K},k_z}(\boldsymbol{r}) = \exp(\mathrm{i}\boldsymbol{K}\cdot\boldsymbol{R})\exp(\mp\gamma z)\cos(\pi z/a \pm \chi) \tag{2.24}$$

where the phase angle χ varies from $+\pi/2$ at the bottom of the gap to 0 at the top if V_g is positive, and between 0 at the bottom and $-\pi/2$ at the top if V_g is negative. Assuming that the crystal potential (2.19) holds right up to the surface at $z = 0$ a surface-state wavefunction must then have the form:

$$\psi_{\boldsymbol{K}}(\boldsymbol{r}) = a\exp(\mathrm{i}\boldsymbol{K}\cdot\boldsymbol{R})\exp(-\gamma z)\cos(\pi z/a + \chi) \qquad z > 0 \tag{2.25}$$

and with a flat vacuum potential:

$$\psi_{\boldsymbol{K}}(\boldsymbol{r}) = b\exp(\mathrm{i}\boldsymbol{K}\cdot\boldsymbol{R})\exp(\gamma' z) \qquad z < 0. \tag{2.26}$$

The logarithmic derivative of ψ on the crystal side of $z = 0$ is given by

$$\frac{1}{\psi_{\boldsymbol{K}}}\frac{\partial\psi_{\boldsymbol{K}}}{\partial z}\bigg|_{z=0} = -\gamma - \frac{\pi}{a}\tan\chi \tag{2.27}$$

which varies between $-\infty$ and $-\gamma$ if V_g is positive, and $-\gamma$ and ∞ if V_g is negative; on the vacuum side the logarithmic derivative is positive. So it is possible to match the wavefunction at some energy in the gap, and hence obtain a surface state, only if V_g is negative (Shockley 1939).

This narrow band gap surface state is called a Shockley state, and the Al (001) surface state shown in figure 4 provides a good example. In a narrow gap the surface state extends relatively deeply into the solid, because γ in (2.25) is small, but more localised states occur in the wider band gaps of semiconductors which correspond to

dangling chemical bonds. Another type of surface state occurs in materials in which the electrons are relatively tightly bound and the wavefunctions have the LCAO/tight-binding form—if the potential at the surface changes enough, a localised state (the Tamm state) is pulled off the band edge (Forstmann 1978).

2.3. *Methods of calculating surface electronic structure*

2.3.1. Wavefunction matching. The first self-consistent calculations were carried out by Lang and Kohn (1970) for the surface of jellium, in which the positive ions are smeared out into a uniform positive background cut off sharply at the surface and the electrons are allowed to redistribute themselves at the surface—this is a good model for the s–p bonded (simple) metals like Na and Al in which the atoms scatter the electrons only weakly. Lang and Kohn matched free-electron bulk wavefunctions (2.11) onto the solution of the Schrödinger equation integrated from the vacuum through the self-consistently determined surface barrier. The surface charge density, potential and surface energy were calculated for a range of jellium densities, corresponding to different metals, and the effects of the weak pseudopotentials included by first-order perturbation theory. These calculations have proved very important, and we shall consider their implications in §§ 3–5.

The full wavefunction matching procedure, including the crystal potential, has been carried out by Appelbaum and Hamann (1972, 1973) for the Na (001) and semiconductor surfaces, matching bulk wavefunctions given by (2.15) onto the solution of the Schrödinger equation in the surface region. At the surface the potential and wavefunctions are expanded as Fourier series over the surface reciprocal lattice vectors:

$$V(\boldsymbol{r}) = \sum_{\boldsymbol{G}} V_{\boldsymbol{G}}(z) \exp(\mathrm{i}\boldsymbol{G} \cdot \boldsymbol{R}) \tag{2.28}$$

$$\psi_{\boldsymbol{K}}(\boldsymbol{r}) = \exp(\mathrm{i}\boldsymbol{K} \cdot \boldsymbol{R}) \sum_{\boldsymbol{G}} u_{\boldsymbol{G}}(z) \exp(\mathrm{i}\boldsymbol{G} \cdot \boldsymbol{R}) \tag{2.29}$$

and substituting into the Schrödinger equation we obtain a set of coupled one-dimensional differential equations:

$$\tfrac{1}{2}|\boldsymbol{K}+\boldsymbol{G}|^2 u_{\boldsymbol{G}}(z) - \frac{1}{2}\frac{\mathrm{d}^2 u_{\boldsymbol{G}}}{\mathrm{d}z^2} + \sum_{\boldsymbol{G}'} V_{\boldsymbol{G}-\boldsymbol{G}'}(z) u_{\boldsymbol{G}'}(z) = E u_{\boldsymbol{G}}(z). \tag{2.30}$$

These can be solved given the asymptotic form of $u_{\boldsymbol{G}}$ in the vacuum:

$$\begin{aligned} u_{\boldsymbol{G}}(z) &\sim b_{\boldsymbol{G}} \exp(\gamma'_{\boldsymbol{G}} z) \qquad z \to -\infty \\ \gamma'_{\boldsymbol{G}} &= [|\boldsymbol{K}+\boldsymbol{G}|^2 + 2(V_0 - E)]^{1/2} \end{aligned} \tag{2.31}$$

and the boundary condition that (2.29) matches onto the bulk solution (2.15) over some plane inside the solid, away from the surface barrier. A major difficulty in these calculations is that the iteration process by which self-consistency is achieved tends to be unstable, because the surface potential barrier is an extremely sensitive function of charge distribution. Appelbaum and Hamann (1972) use a straightforward iteration procedure in which only a fraction of the output potential $U_n(\boldsymbol{r})$ from the charge density in the nth iteration is used to construct the input potential $V_{n+1}(\boldsymbol{r})$ for the $(n+1)$th iteration:

$$V_{n+1}(\boldsymbol{r}) = (1-\alpha) V_n(\boldsymbol{r}) + \alpha U_n(\boldsymbol{r}). \tag{2.32}$$

More complicated procedures can be used to speed convergence, and Lang and Kohn (1970) expand the correction to an approximate charge density in a basis set, with coefficients determined by considering the linear response to this correction.

The wavefunction matching approach has been widely used with a non-self-consistent step potential at the surface in LEED calculations (Pendry 1974) in which an electron is incident on the surface, and the waves reflected into vacuum must be found. It has also been used in field-emission calculations (Nicolaou and Modinos 1975), in which the potential in the surface region includes the effects of the applied electric field.

2.3.2. Green functions and tight binding. Wavefunction matching methods are not ideal for surfaces, as the wavefunctions usually contain more information than we need, and are not local properties like $\sigma(\boldsymbol{r}, E)$ (2.16). σ is closely related to the Green function, which satisfies the inhomogeneous Schrödinger equation:

$$(-\tfrac{1}{2}\nabla_r^2 + V(\boldsymbol{r}) - E)G(\boldsymbol{r}, \boldsymbol{r}'; E) = \delta(\boldsymbol{r} - \boldsymbol{r}'). \tag{2.33}$$

The formal solution of (2.33) can be written in terms of eigenfunctions and eigenvalues of the corresponding homogeneous equation:

$$G(\boldsymbol{r}, \boldsymbol{r}'; E) = \sum_i \frac{\psi_i^*(\boldsymbol{r})\psi_i(\boldsymbol{r}')}{\epsilon_i - E} \tag{2.34}$$

so the local density of states is given by

$$\sigma(\boldsymbol{r}, E) = \frac{1}{\pi} \operatorname{Im} G(\boldsymbol{r}, \boldsymbol{r}; E + \mathrm{i}\delta). \tag{2.35}$$

The Green function, hence σ, is particularly easy to calculate in tight-binding systems in which the atomic orbitals do not overlap very much, as in the 3d, 4d or 5d bands of the transition metals. In the tight-binding/LCAO approach the atomic orbitals (or some other localised orbitals) are used as basis functions, and we consider matrix elements of the Green function operator $(H - E)^{-1}$:

$$G_{\alpha,I;\beta,J}(E) = \langle \alpha, I | (H - E)^{-1} | \beta, J \rangle \tag{2.36}$$

where $|\alpha, I\rangle$ corresponds to an orbital of type α on atom I. The equivalent of (2.35) in the orbital representation is then

$$\sigma_{\alpha,I}(E) = \frac{1}{\pi} \operatorname{Im} \langle \alpha, I | (H - E - \mathrm{i}\delta)^{-1} | \alpha, I \rangle \tag{2.37}$$

i.e. the charge density in orbital $|\alpha, I\rangle$ at energy E. This can be evaluated entirely in real space, in terms of an electron hopping from one atom to the next, without any consideration of wavefunctions (Heine 1980). One way to do this is to calculate the moments of $\sigma_{\alpha,I}(E)$ (Cyrot-Lackmann 1969), the nth moment being defined as

$$\begin{aligned} \mu_{\alpha,I}^{(n)} &= \int_{-\infty}^{\infty} \mathrm{d}E\, E^n \sigma_{\alpha,I}(E) \\ &= \frac{1}{\pi} \operatorname{Im} \int_{-\infty}^{\infty} \mathrm{d}E\, E^n \langle \alpha, I | (H - E - \mathrm{i}\delta)^{-1} | \alpha, I \rangle. \end{aligned} \tag{2.38}$$

Knowing all the moments, $\sigma_{\alpha,I}(E)$ is determined uniquely. Using contour integration we write (2.38) as

$$\mu_{\alpha,I}^{(n)} = \frac{1}{2\pi i}\oint dE\, E^n \langle \alpha, I|(H - E - i\delta)^{-1}|\alpha, I\rangle \tag{2.39}$$

where the contour encloses all the poles just below the real axis in a clockwise direction, and then from Cauchy's integral formula we obtain

$$\mu_{\alpha,I}^{(n)} = \langle \alpha, I|H^n|\alpha, I\rangle. \tag{2.40}$$

This can be evaluated very simply by writing H^n in full as $HHH\ldots$ and inserting the set of states $\Sigma_{\beta,J}|\beta, J\rangle\langle\beta, J|$—the unit matrix in this representation—between every pair of H:

$$\mu_{\alpha,I}^{(n)} = \sum_{\beta,J}\sum_{\gamma,K}\ldots\sum_{\lambda,L}\langle\alpha, I|H|\beta, J\rangle\langle\beta, J|H|\gamma, K\rangle\ldots\langle\lambda, L|H|\alpha, I\rangle. \tag{2.41}$$

Each term in this summation is just a product of n hopping integrals, or self-energies $\langle\alpha, I|H|\alpha, I\rangle$, taking us in n steps from orbital $|\alpha, I\rangle$ out into the crystal and back again; by enumerating all these paths of n steps we can find the nth moment. The finer details of $\sigma_{\alpha,I}(E)$ correspond to the high moments, and we see from (2.41) that these depend on probing the environment more and more deeply.

As this is a real space method it is particularly suitable for surfaces, where there is no translational symmetry in the z direction. The French school have applied the method of moments widely to find the surface density of states for transition metals (Desjonquères and Cyrot-Lackmann 1975), using fitted hopping parameters, and including intra-atomic potential shifts to take rough account of self-consistency. An alternative real space approach is based on the tridiagonalisation of the tight-binding Hamiltonian matrix (Haydock 1980), and this has been applied to similar problems (Kelly 1980). The drawback of tight binding is that the Hamiltonian is not particularly accurate, and it is difficult to take proper account of self-consistency.

2.3.3. Slab calculations. The most widely used approach for accurate calculations of the surface electronic structure is to consider a finite slab, with two surfaces separated by a sufficient thickness of bulk material that each is representative of the surface of a semi-infinite crystal. It is ironic that we fall back on this approach, having constructed the formal apparatus of finding wavefunctions in a semi-infinite crystal in § 2.2, but it gives a finite problem and we can use standard basis function methods for solving the Schrödinger equation.

In one approach the slabs are periodically repeated in the z direction, with vacuum in between, giving a three-dimensional 'crystal' with a very large unit cell in the z direction (Schlüter *et al* 1975). The wavefunctions can then be characterised by a three-dimensional Bloch wavevector $\boldsymbol{k}$, and can be expanded in plane waves; this has been applied to metal and semiconductor slabs, replacing the deep ion-core potentials by much weaker pseudopotentials to improve convergence. Even so, the problem is very large, and in a typical calculation on nine-layer Nb (001) slabs, with a slab–slab separation of six atomic spacings, about 1000 plane waves must be used (Louie *et al* 1977). Alternatively, localised orbitals can be used as basis functions for an isolated slab (Wang and Freeman 1979). The basis functions are usually taken from numerical solutions of the Schrödinger equation for an isolated atom, and unlike in tight-binding calculations (§ 2.3.2) the matrix elements of the Hamiltonian are properly evaluated.

An approach which has the advantage of localised orbitals in coping well in the core region of atoms, and of plane waves in working well between atoms, is the linear augmented plane wave (LAPW) method (Jepsen *et al* 1978, Krakauer *et al* 1979a). For the purpose of constructing the basis functions, the slab is divided into three regions: muffin tins containing the ion-core potentials, the interstitial region between

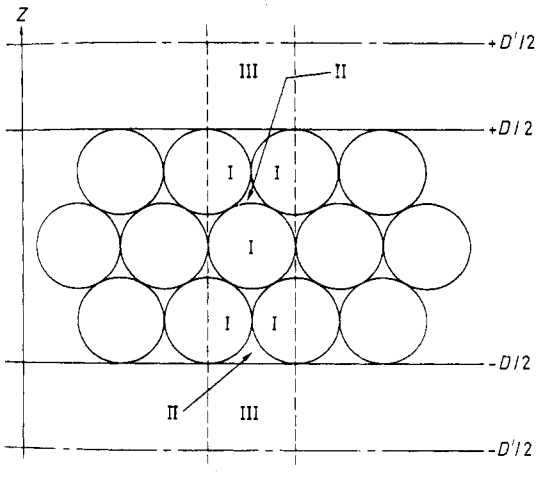

Figure 5. Slab geometry for LAPW calculations. The slab is divided into three regions: I, muffin-tin spheres; II, interstitial region; III, vacuum region (Krakauer *et al* 1979a).

atoms and a vacuum region extending out from the surfaces of the slab (figure 5). In the interstitial region the basis functions are sines or cosines:

$$\varphi_{\boldsymbol{K},\boldsymbol{G},n}(\boldsymbol{r}) = \exp\left[\mathrm{i}(\boldsymbol{K}+\boldsymbol{G})\cdot\boldsymbol{R}\right]\begin{cases}\cos k_n z\\ \sin k_n z\end{cases} \tag{2.42}$$

where the wavevectors k_n are chosen so that φ goes to zero on some plane outside the slab. Inside the muffin tins, the Schrödinger equation is integrated outwards (with a spherically symmetric potential) at some chosen energy, to give the radial function $u_l(\boldsymbol{r})$ and its energy derivative $\dot{u}_l(\boldsymbol{r})$; a linear combination of the u_l and $\dot{u}_l$ is then taken:

$$\varphi_{\boldsymbol{K},\boldsymbol{G},n}(\boldsymbol{r}) = \sum_L \left[A_{L,\boldsymbol{K}+\boldsymbol{G},n}u_l(\boldsymbol{r}) + B_{L,\boldsymbol{K}+\boldsymbol{G},n}\dot{u}_l(\boldsymbol{r})\right] Y_L(\Omega) \tag{2.43}$$

such that (2.43) matches in both amplitude and derivative onto (2.42) on the surface of the muffin tins. Similarly in the vacuum region the basis function is given by

$$\varphi_{\boldsymbol{K},\boldsymbol{G},n}(\boldsymbol{r}) = \exp\left[\mathrm{i}(\boldsymbol{K}+\boldsymbol{G})\cdot\boldsymbol{R}\right]\left[C_{\boldsymbol{K}+\boldsymbol{G},n}v_{\boldsymbol{K},\boldsymbol{G}}(z) + D_{\boldsymbol{K}+\boldsymbol{G},n}\dot{v}_{\boldsymbol{K},\boldsymbol{G}}(z)\right] \tag{2.44}$$

where v satisfies the Schrödinger equation for an x–y averaged vacuum potential, $\dot{v}$ is its energy derivative, and the linear combination is again chosen so that (2.44) matches onto (2.42) on the boundary of the vacuum region. This is a very good way of constructing the basis set, because u, $\dot{u}$, v, $\dot{v}$ provide an accurate solution of the Schrödinger equation in their respective regions over quite a wide energy range around the fixed energy parameter (Krakauer *et al* 1979a), and the wavefunction and its derivative are continuous across the boundaries between regions (unlike the APW method) (Ziman 1972). Moreover, the matrix elements of the full Hamiltonian can be found very readily. This makes the LAPW method seem well suited to self-consistent slab calculations, and the results to date are encouraging.

Self-consistent slab calculations represent the present state of the art of finding the surface electronic structure, but they are not the last word: the bulk and surface-state wavefunctions are not clearly separated, and with a thin slab (the typical thickness is only seven layers) there must be some interaction between the surfaces. This lack of separation between the bulk and surface properties also makes it difficult to extract the surface energy from such calculations.

2.3.4. Other methods. One method which has been applied to a wide range of problems is the matching Green function method (Inglesfield 1978a, b), in which the Green function for an atom at the surface is constructed from Green functions for the isolated atom and substrate. Although it is difficult to use this method self-consistently it gives reasonable densities of states if a good potential is used in the surface atom (Inglesfield 1979a). The method is also useful in model calculations, and in calculations of linear response functions (Inglesfield 1979b) which can be expressed in terms of $G(\boldsymbol{r}, \boldsymbol{r}'; E)$. We have reviewed this method, and other methods of calculating the surface electronic structure elsewhere (Inglesfield and Holland 1981).

3. Surface electronic structure of metals and semiconductors

Detailed calculations of surface electronic structure, which we shall review in this section, show characteristic effects in the local density of states. The surface density of states shows a reduction in weight at band edges compared with the bulk, band narrowing in transition metals, and different types of surface states—all effects which can be understood in terms of the different environment of the surface atoms. In wide band gap semiconductors and insulators, where local chemical bonds can be used, the surface states have a direct interpretation as dangling bonds. By the second layer of atoms, the local density of states and the charge density are already close to the bulk values, because the atoms are now in a bulk-like environment.

The effects of the surface are most marked at band edges (always the least local region of local densities of states), and we saw in figure 4 that $n_{s,\boldsymbol{K}}(E)$ has an $|E-\epsilon_0|^{1/2}$ singularity rather than the $|E-\epsilon_0|^{-1/2}$ singularity of the bulk density of states at fixed wavevector $\boldsymbol{K}$ (Inglesfield 1978a). The energy band edge ϵ_0 is a quadratic function of K around an extremum in the full three-dimensional bulk density of states, and integrating over $\boldsymbol{K}$, the surface density of states at the bottom of the band, for example, varies like

$$n_s(E) = \int K \, dK \, (E - \alpha K^2)^{1/2}$$

$$\sim E^{3/2}. \tag{3.1}$$

The surface density of states rises more gradually than the bulk density of states, which varies like $E^{1/2}$ at this band edge. This is shown very clearly in figure 6 which gives $\sigma(z, E)$, the local density of states integrated over $\boldsymbol{K}$, for a self-consistent jellium potential, as a function of E at different distances z from the surface (Werner *et al* 1975). σ rapidly approaches the bulk density of states as we move in from the surface, though at any finite distance from the surface it varies like $E^{3/2}$ right at the band edge.

The removal of weight at band edges gives rise to band narrowing in an isolated band of states (Cyrot-Lackmann 1969). The local density of states at the surface of a simple cubic crystal with a tightly bound s band (Haydock and Kelly 1973) is shown

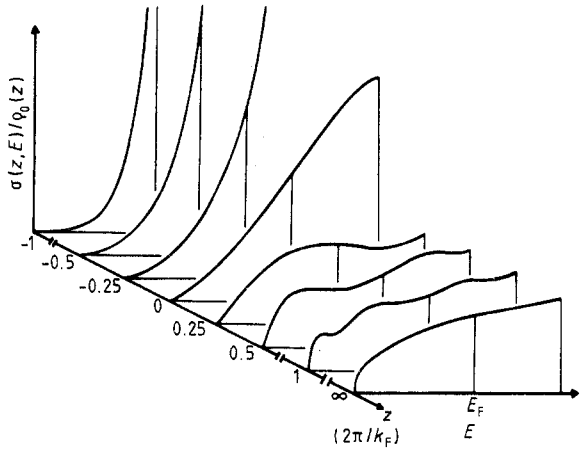

Figure 6. $\sigma(z, E)$ (normalised by charge density $\rho_0(z)$) as a function of E at different distances from the surface; calculated for Lang–Kohn potential at $r_s = 4$ au (Werner *et al* 1975).

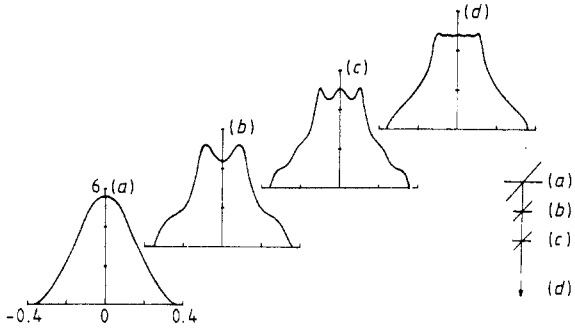

Figure 7. Local density of states $n_s(E)$ on (001) surface (a) and sub-surface (b)–(d) atoms of simple cubic s-band solid (Haydock and Kelly 1973).

in figure 7, and we see once again that the $E^{1/2}$ behaviour of the bulk density of states at the band extrema becomes $E^{3/2}$ at the surface, with weight being transferred to the centre of the band. This band narrowing at the surface can be understood very easily using the method of moments which we discussed in § 2.3.2: the second moment of $\sigma_I(E)$ measures its mean square width, and from (2.41) this is given by

$$\mu_I^{(2)} = nh^2 \tag{3.2}$$

where n is the number of neighbours of atom I and h is the hopping integral. But n is smaller for a surface atom than for one in the bulk, so the local density of states must be narrower (Kelly 1980)—this is found in the tightly bound d bands on transition-metal surfaces. From figure 7 we see that the local density of states goes rapidly to the bulk value, and even on the second layer it is quite close.

The changes in the local density of states at a narrow band gap in the band structure depend on whether or not a Shockley surface state occurs, because *the surface state removes weight from the neighbouring band edges.* We can show this very clearly by considering changes in the *integrated* density of states: we define $N_{\boldsymbol{K}}(E)$, the integrated density of states, as the total number of states in the specimen with wavevector $\boldsymbol{K}$

and energy less than E, i.e.

$$N_{\boldsymbol{K}}(E) = \int^{E} \mathrm{d}E \int \mathrm{d}\boldsymbol{r}\, \sigma_{\boldsymbol{K}}(\boldsymbol{r}, E). \tag{3.3}$$

The change in $N_{\boldsymbol{K}}(E)$ due to a surface, $\delta N_{\boldsymbol{K}}(E)$, can be found directly using the matching Green function method without explicit integration of $\sigma_{\boldsymbol{K}}$ (Inglesfield 1978a). Figure 8 shows $\delta N_{\boldsymbol{K}}(E)$ for the surface of a free-electron metal with a one-dimensional

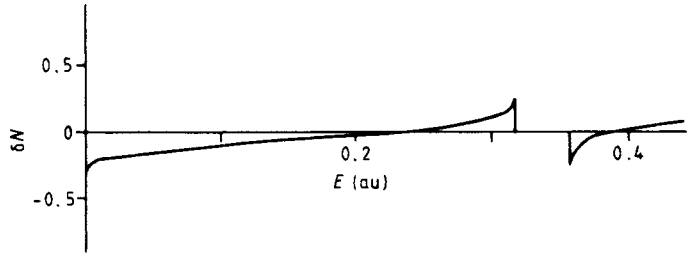

Figure 8. $\delta N_{\boldsymbol{K}=0}(E)$, with $V_g = +0.02$ au and no surface state.

potential (2.19); taking π/a to be 0.822 au and the single Fourier component of the potential $V_g = +0.02$ au there is a band gap at $\boldsymbol{K} = 0$ between $E = 0.32$ and 0.36 au, not containing a surface state as V_g is positive. We see first that $\delta N_{\boldsymbol{K}}(E)$ has discontinuities corresponding to *the loss of* $\frac{1}{4}$ *state at each band edge*—a completely general result due to the $|E - \epsilon_0|^{1/2}$ variation of $\sigma_{\boldsymbol{K}}(\boldsymbol{r}, E)$ in the presence of a surface (Inglesfield 1978a). However, the loss altogether of $\frac{1}{2}$ state at the band gap tends to be compensated by an increase in the number of states away from the gap. The situation is quite different when V_g is negative and a surface state occurs, and taking $V_g = -0.02$ au (the parameters are appropriate to Al) we obtain $\delta N_{\boldsymbol{K}}(E)$ shown in figure 9: the surface state at $E = 0.335$ au leads to a further reduction in states around the band gap, in addition to the $\frac{1}{4}$ state lost at each band edge. These changes in $\delta N_{\boldsymbol{K}}(E)$ correspond to changes in $\sigma_{\boldsymbol{K}}(\boldsymbol{r}, E)$ which are relatively localised at the surface except for the very long-range behaviour right at the band edge.

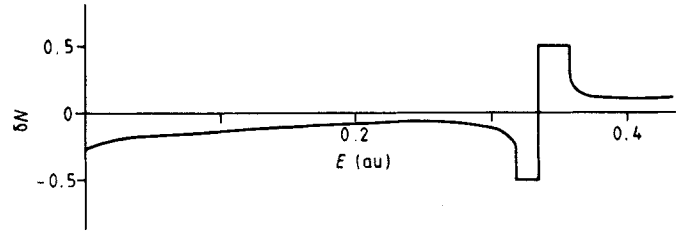

Figure 9. $\delta N_{\boldsymbol{K}=0}(E)$, with $V_g = -0.02$ au.

The effect of the surface state on the local density of states can be seen in figure 4 where it compensates for the reduction in $n_{s,\boldsymbol{K}}(E)$ compared with the bulk density of states around the band gap. On the other hand, the reduction in weight at the bottom of the band is compensated for by an increase in $n_{s,\boldsymbol{K}}$ at $E \approx 0.1$ au. The overall result is that the surface density of states is quite close to the bulk density of states, not surprising because the atoms on the Al (001) surface still have 8 of the 12 bulk nearest neighbours.

3.1. Surfaces of simple metals

Because the pseudopotentials are weak and the band structures are nearly-free-electron-like, a good approximation for s–p bonded (simple) metal surfaces is the jellium model in which a uniform positive background is cut off sharply at the surface. Self-consistent charge densities calculated in this model by Lang and Kohn (1970) are shown in figure 10 for bulk electron densities of $r_s = 2$ au (corresponding to Al)

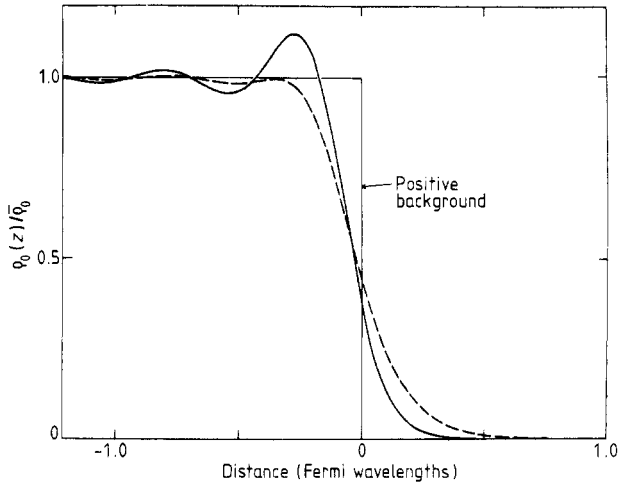

Figure 10. Self-consistent charge density, in uniform positive background model of a metal surface, $r_s = 2$ (– – –) and 5 (——) au (Lang and Kohn 1970).

and $r_s = 5$ au (corresponding to K). The charge density $\rho_0(z)$ shows Friedel oscillations, which always occur when a perturbation is applied to a free-electron gas (Ziman 1972); these vary asymptotically like (Lang and Kohn 1970)

$$\delta\rho_0(z) \sim \frac{\alpha \cos[2(k_F z + \chi)]}{(2k_F z)^2} \tag{3.4}$$

where k_F is the Fermi wavevector and χ is the phase shift in an incident wave at the Fermi level reflected by the surface ((2.11) can be rewritten as 2 exp ($i\boldsymbol{K} \cdot \boldsymbol{R}$) cos [$k_z z + \chi(k_z)$]). In the case of Al the oscillations are very small, much smaller than in a non-self-consistent jellium calculation with a step potential at the surface, and even in the low-density case where there is a large overshoot in ρ_0 at the first oscillation, the charge density has settled down to practically its bulk value within half a Fermi wavelength of the surface. The jellium calculations can be used to find work functions (Lang and Kohn 1971) (§ 4) and surface energies (Lang and Kohn 1970) (§ 5), and when the effects of the pseudopotential are included by first-order perturbation theory, good results are obtained for the whole range of simple metals.

Self-consistent calculations in which the ionic potentials are included from the start have been carried out, using wavefunction matching (Appelbaum and Hamann 1972) (§ 2.3.1), slab methods (Wang *et al* 1981, Ley *et al* 1981) (§ 2.3.3) and density matrix techniques (Bohnen and Ying 1980), for the alkalis, the alkaline earths and Al. In all cases the charge density is similar to the jellium results (figure 11), though the Friedel oscillations are modified by the screening of the ion cores; by the second layer of atoms it is close to the bulk value. The results for Al (111) (Wang *et al*

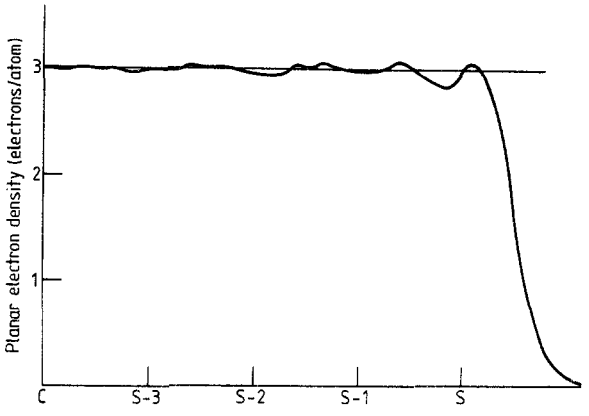

Figure 11. Planar averaged valence electron density at Al (111) surface (Wang *et al* 1981).

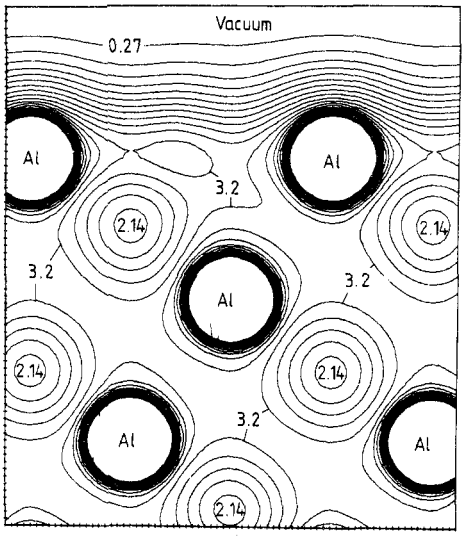

Figure 12. Contours of charge density at Al (111) surface (Wang *et al* 1981).

1981) (figure 12) provide an example of the *smoothing of the surface charge density* compared with a superposition of atomic charge densities. The charge distribution at a surface is a result of competition between the potential energy, which tries to draw the electrons into the region where the potential is strong, and the kinetic energy which tends to spread the electrons out—the smoothing at the surface, a general feature of surface charge redistribution, lowers the kinetic energy. We shall see in § 4 that it is an important effect in determining work function variations from surface to surface. These fully self-consistent calculations automatically give the work function φ, the energy needed to remove an electron at the Fermi energy from the solid. For Na (001) (Appelbaum and Hamann 1972, Bohnen and Ying 1980) theory gives $\varphi = 2.7$ eV, in perfect agreement with experiment, and for Al (111) (Wang *et al* 1981, Chelikowsky *et al* 1975) the theoretical values are 4.73 eV and 5.2 eV, compared with the experimental value of 4.26 eV; some of the discrepancy in the case of Al may be due to the choice of exchange-correlation potential (§ 2.1).

3.1.1. Surface states on Al. A surface state shows up strongly in angle-resolved photoemission experiments on Al, appearing as a sharp peak in the emission intensity as a function of the photoelectron energy (Hansson and Flodström 1978) (figure 13).

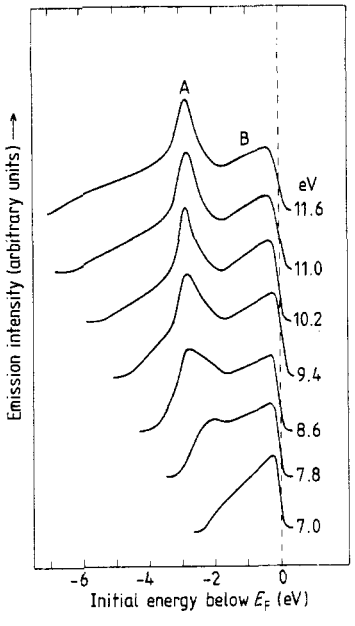

Figure 13. Intensity of electrons photoemitted normal to Al (001) for different photon energies. Peak A corresponds to the surface state (Hansson and Flodström 1978).

As the wavevector parallel to the surface is conserved in photoemission, different angles of emission correspond to different values of $\boldsymbol{K}$ for the initial state, and in this way the dispersion of the surface state through the surface Brillouin zone can be measured: figure 14 shows the dispersion of the Al (001) surface state for $\boldsymbol{K}$ in the $\bar{\Gamma}\bar{M}$ and $\bar{\Gamma}\bar{X}$ directions, together with the band gap in the bulk band structure (Hansson and Flodström 1978). Detailed calculations have been made of the Al (001) surface electronic structure which show the surface state (figure 4) (Caruthers *et al* 1973,

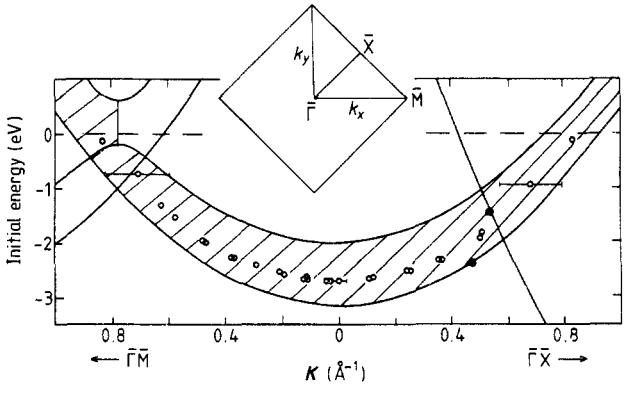

Figure 14. Dispersion of Al (001) surface state as a function of $\boldsymbol{K}$ in $\bar{\Gamma}\bar{M}$ and $\bar{\Gamma}\bar{X}$ directions of surface Brillouin zone. Full lines show bulk band edges (Hansson and Flodström 1978).

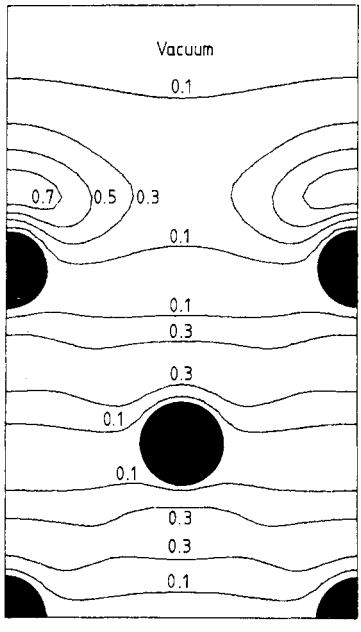

Figure 15. Contours of charge density of Al (001) surface state with $\boldsymbol{K} = 0$ (Krakauer *et al* 1981).

Krakauer *et al* 1981), and figure 15 shows its charge density from a self-consistent slab calculation. The occurrence and character of this surface state can be understood using the simple theory of Shockley surface states given in § 2.2. The band gap is due to the pseudopotential component corresponding to the bulk reciprocal lattice vector $\boldsymbol{g} = 2\pi/a\ (0, 0, 2)$, and with respect to an origin halfway between atomic planes V_g is negative, -0.02 au (Hansson and Flodström 1978), so the criterion for the occurrence of a Shockley surface state is satisfied. As V_g is negative electronic states which pile up charge between atomic planes (p-like states) have a lower energy than s states which pile up charge on the atoms; however, it is inappropriate to think of chemical bonds in Al and the surface state is not a dangling bond, even though the charge density is greatest outside the surface (figure 15). We see from this figure that the surface state dies away only slowly into the solid, and in nearly-free-electron theory its decay constant is given by

$$\gamma = |V_g|/(g/2) = 0.024 \text{ au} \tag{3.5}$$

corresponding to a decay length of about 20 atomic layers.

The band gap is absolute for $\boldsymbol{K}$ around the $\bar{\Gamma}$ point at the centre of the surface Brillouin zone, but as we move towards the edge of the zone, other bulk bands start crossing it and complicate our simple surface-state picture. Figure 16(a) shows the bulk Al band structure as a function of k_z for several points between $\bar{\Gamma}$ and $\bar{\mathrm{M}}$ with $\boldsymbol{K} = (K, 0)$. At small K they show quite clearly the band gap at $k_z = 2\pi/a$ coming from the interaction between plane waves $\exp(\mathrm{i}\boldsymbol{K}x)\exp(\mathrm{i}k_z z)$ and $\exp(\mathrm{i}\boldsymbol{K}x)\exp[\mathrm{i}(k_z - 4\pi/a)z]$, with other bands well removed in energy. But as K increases, two other bands approach the band gap, coming from plane waves displaced from $\boldsymbol{k} = (K, 0, k_z)$ by the bulk reciprocal lattice vectors $\boldsymbol{g} = 2\pi/a\ (1, 1, 1)$ and $2\pi/a\ (1, \bar{1}, 1)$:

$$\begin{aligned} \varphi_{111} &= \exp\{\mathrm{i}[(K - 2\pi/a)x - 2\pi y/a]\}\exp[\mathrm{i}(k_z - 2\pi/a)z] \\ \varphi_{1\bar{1}1} &= \exp\{\mathrm{i}[(K - 2\pi/a)x + 2\pi y/a]\}\exp[\mathrm{i}(k_z - 2\pi/a)z]. \end{aligned} \tag{3.6}$$

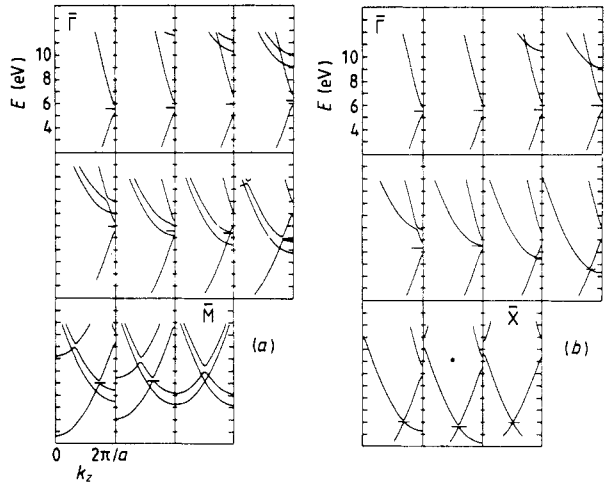

Figure 16. Al band structure as a function of k_z: (*a*) $\boldsymbol{K}$ between $\bar{\Gamma}$ and $\bar{M}$ in (001) surface Brillouin zone; (*b*) $\boldsymbol{K}$ between $\bar{\Gamma}$ and $\bar{X}$ (Spanjaard *et al* 1979).

The (0, 2, 0) component of the pseudopotential mixes these two plane waves together forming the linear combinations:

$$\begin{aligned}\varphi_+ &= \exp[\mathrm{i}(K-2\pi/a)x]\cos(2\pi y/a)\exp[\mathrm{i}(k_z-2\pi/a)z]\\ \varphi_- &= \exp[\mathrm{i}(K-2\pi/a)x]\sin(2\pi y/a)\exp[\mathrm{i}(k_z-2\pi/a)z]\end{aligned} \tag{3.7}$$

which are split in energy by $2|V_{020}|$. As V_{020} is positive with respect to an origin on the atoms, the sine combination φ_- has the lower energy, and meets the bottom of our band gap at $K=\pi/a$, halfway to $\bar{M}$ (figure 16(*a*)). But φ_- is antisymmetric with respect to reflection in the $y=0$ plane, whereas the surface state which has the wavefunction (2.25):

$$\psi = \exp(\mathrm{i}Kx)\exp(-\gamma z)\cos(2\pi z/a+\chi) \tag{3.8}$$

is symmetric. So the surface state cannot interact with φ_- and leak away into it, even though it has the same energy as this bulk state. The photoemission results go a little beyond $K=\pi/a$ before the surface state moves up through the Fermi energy, and confirm that the state remains sharp (Hansson and Flodström 1978).

In the $\bar{\Gamma}\bar{X}$ direction, on the other hand, mixing with a bulk band can take place. In this direction, $\boldsymbol{K}=(K,K)$, the band arising from the plane wave:

$$\varphi_{111} = \exp\{\mathrm{i}[(K-2\pi/a)x+(K-2\pi/a)y]\}\exp[\mathrm{i}(k_z-2\pi/a)z] \tag{3.9}$$

meets the band gap about halfway to $\bar{X}$ (figure 16(b)), and now there are no symmetry restrictions preventing its interaction with the surface state. Indeed we see that there is a splitting when this band crosses the two bands $\exp[\mathrm{i}(Kx+Ky)]\exp(\mathrm{i}k_z z)$ and $\exp[\mathrm{i}(Kx+Ky)]\exp[\mathrm{i}(k_z-4\pi/a)z]$ which give rise to the gap and the surface state. Beyond this point a true surface state can no longer occur, as electrons can leak into the bulk band carrying flux into the crystal. Nevertheless a peak is still observed in the photoemission results (figure 14) (Hansson and Flodström 1978) and in calculations of the surface density of states (Krakauer *et al* 1978, Inglesfield and Holland 1981): the surface state has become a *surface resonance*, with a wavefunction extending into the bulk, but peaked at the surface.

The band gap due to the $\boldsymbol{g} = 2\pi/a$ (0, 0, 2) component of the pseudopotential can give rise to surface states on other surfaces besides the (001), if it remains an absolute gap when projected in these other directions. Figure 17, for example, shows the

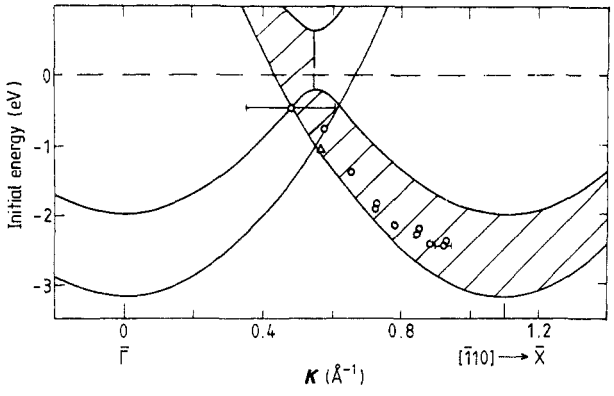

Figure 17. Dispersion of Al (110) surface state. The shaded area shows the projected band gap around X in the bulk band structure (Hansson and Flodström 1978, 1979).

dispersion of an Al (110) surface state measured by angle-resolved photoemission around $\bar{X}$ in the surface Brillouin zone (Hansson and Flodström 1978, 1979). The surface state lies in the projection of the (2, 0, 0) and (0, 2, 0) band gaps in this direction, and as it comes from the same energy gap, its wavefunction is closely related to the (001) surface-state wavefunction (Inglesfield and Holland 1981). This is an example of the 'transferability' of surface states from one surface to another, which is also found on transition-metal surfaces (Holmes and Inglesfield 1979). A slab calculation by Caruthers *et al* (1974) predicted the surface state at $\bar{X}$ on Al (110), together with a state at $\bar{\Gamma}$ coming from another band gap which also seems to show up in the photoemission experiments.

3.1.2. Surface states on other simple metals. The band gaps in the alkali metals lie above the Fermi energy, and a self-consistent slab calculation for the (001) surface of BCC† Li gives unoccupied surface states above E_F but below the vacuum level (Alldredge and Kleinman 1974). Such states will not show up in photoemission experiments, of course, but there are techniques for measuring unoccupied states, such as appearance potential spectroscopy in which an incident electron drops down to an unoccupied state and at the same time excites a core electron (Park and Houston 1972). The probability for creating the core hole thus depends on a convolution of densities of unoccupied states, and can be measured from the soft x-ray or Auger electron emission as it decays (Park 1979). This has been used to study unoccupied states in the oxidation of Ca, Sr and Ba (Nyberg 1977). Recently it has been shown that the inverse photoemission process can be used to study unoccupied bands at surfaces (Pendry 1980b, Denninger *et al* 1982): a low-energy electron incident on a surface drops into an unoccupied level and emits a photon. As the mean free path of the incident electron is short, and the matrix element for the process is the same as in photoemission, inverse photoemission provides a surface-sensitive technique for probing the energy and dispersion of the unoccupied states (§ 3.2.3). So far the

† Body-centred cubic.

unoccupied surface state on Li remains unstudied experimentally, but inverse photoemission offers good prospects for observing it.

Features in the photoemission spectra from polycrystalline Ca, Sr and Ba have been identified as surface states by comparison with self-consistent slab calculations (Ley *et al* 1981). Around $\bar{\Gamma}$ in the Ca (001) surface Brillouin zone a surface state is found in the (0, 0, 2) band gap (figure 18); this gap is much wider than in Al because

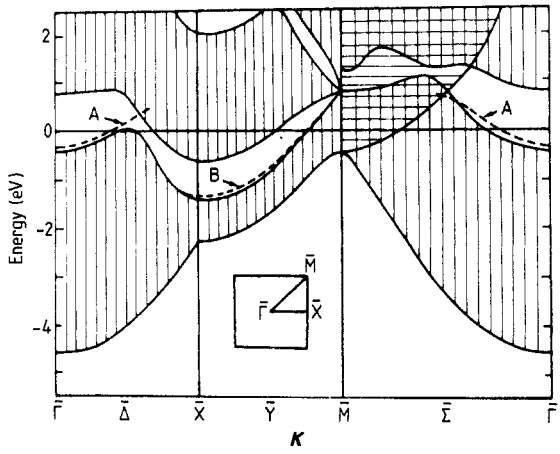

Figure 18. Surface states on Ca (001) with projected band structure (Ley *et al* 1981).

there is hybridisation between the s–p free-electron band and the 3d level above the Fermi energy (McCaffrey *et al* 1973). A bulk band structure calculation shows that the state at the bottom of the energy gap is a mixture of s and d orbitals, the p-like state having higher energy—this shows that the surface state is not a simple narrow band gap state to which we can apply the theory of (2.20)–(2.27).

3.2. Surfaces of transition metals

The surfaces of transition metals are extensively studied, because of the wide range of phenomena they show and their importance industrially as catalysts. Their electronic structure is dominated by the d electrons, as in the bulk where the band structure consists of five narrow d bands hybridising with the s–p band (figure 19). The

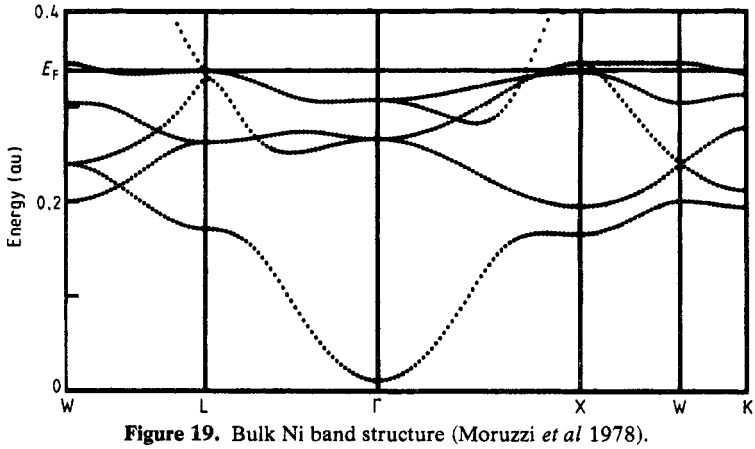

Figure 19. Bulk Ni band structure (Moruzzi *et al* 1978).

tight-binding method (§ 2.3.2) is useful for understanding the behaviour of the d electrons at the surface (Cyrot-Lackmann 1969), though it has now been largely superseded by self-consistent slab calculations for quantitative work.

3.2.1. Mo and W surfaces. Because of the reduction in the number of neighbours, the d bands are narrowed on surface atoms (3.2), and this is particularly marked on the open (001) surface of BCC metals like Mo and W, where each atom has only four nearest neighbours compared with eight in the bulk. Figure 20 shows the results of

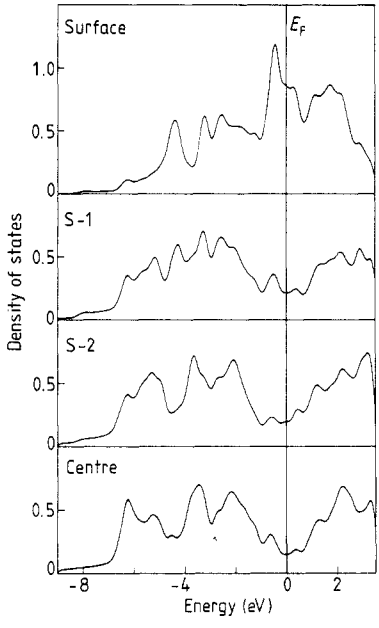

Figure 20. $n_s(E)$ for W (001) in seven-layer slab calculation, compared with densities of states on sub-surface layers. The central peak is apparent, in a minimum in the bulk (central layer) density of states (Posternak *et al* 1980).

a slab calculation of the surface density of states for W (001) (Posternak *et al* 1980), and the main effect of the band narrowing is a characteristic central peak, coinciding with a minimum in the bulk density of states; the density of states at the Mo (001) surface is similar (Kerker *et al* 1978). This peak coincides with the Fermi energy—in fact, the stability of the BCC structure of W and Mo is due to E_F lying in the minimum in the bulk density of states (Pettifor 1970), which is roughly analogous to a band gap between bonding and antibonding states (there is indeed some evidence for directional bonding effects in BCC transition metals, with charge in the d_{xy}, d_{yz} and d_{zx} orbitals tending to pile up between atoms (Zunger *et al* 1979)). We shall see in § 6.2 that the peak at E_F in n_s is probably responsible for the instability of the ideal W and Mo (001) surfaces. The peak can be thought of as a virtual bound d state on the surface atoms (Friedel 1976): it reflects the environment of the surface atoms midway between the isolated atom and the bulk. As we would expect on general grounds, the local density of states on the second layer of atoms is very similar to the bulk (figure 20), because the local environment is the same.

The charge density at the W (001) surface is shown in figure 21 (Posternak *et al* 1980), and already by the second layer of atoms it is very close to the bulk with the

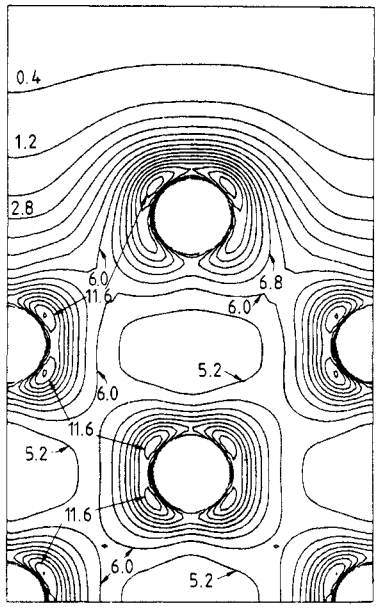

Figure 21. Contours of charge density at W (001) surface (Posternak *et al* 1980).

lobes in the bonding directions plainly visible. Weight is removed from the bonding lobes at the surface, and there is some tendency towards charge density smoothing, though not very effective on this open surface. This calculation gives a value of 4.5 eV for the W (001) work function, compared with the experimental value of 4.6 eV (Posternak *et al* 1980); for Mo (001) Kerker *et al* (1978) obtain $\varphi = 4.3$ eV, compared with the experimental $\varphi = 4.6$ eV. The self-consistent potential also gives immediately any shift in the binding energy of the core levels on the surface atoms, a quantity which can be measured using x-ray photoemission. The calculation for W (001) predicts no surface core shift, in agreement with simple tight binding theory (Posternak *et al* 1980): as a small transfer of charge leads to a large shift in potential, the surface atoms should be almost neutral; because of band narrowing this is achieved by a downward shift in potential (greater binding energy of the core level) if the d band is less than half full, an upward shift if it is more than half full, and no change in the case of W and Mo (Feibelman *et al* 1979). Recent experiments on W show, in fact, an upward shift of 0.30 eV on (110) (Duc *et al* 1979) and 0.35 eV on the (001) surface (van der Veen *et al* 1981). Some of the discrepancy may be due to the effects of screening the core hole in photoemission, which is presumably different at the surface and in the bulk.

3.2.2. Surface states on Mo and W (001) surfaces. The central peak in the surface density of states is made up of surface states and resonances over the whole of the surface Brillouin zone, which tend to occur at this energy. These include a surface state at the centre of the surface Brillouin zone (figure 22) which shows up very strongly in photoemission experiments at −0.3 eV relative to the Fermi energy on Mo (001) and −0.4 eV on W (001) (Weng *et al* 1978). The W (001) state was, in fact, the first surface state to be detected, observed with both field emission (Plummer and Gadzuk 1970) and photoemission (Waclawski and Plummer 1972) (it is ideal for field emission, being close to E_F and having $\boldsymbol{K} = 0$). At first it was assumed that this

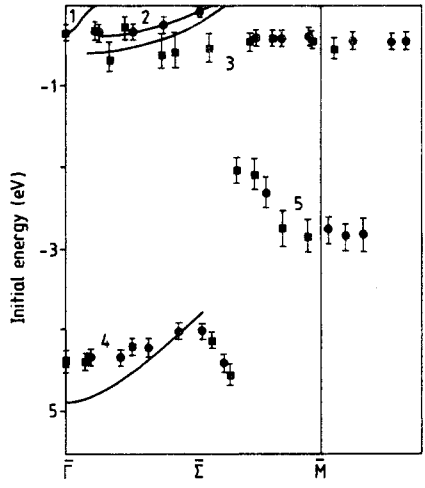

Figure 22. Full curves: calculated dispersion of surface states and resonances on W (001) (Posternak *et al* 1980). The data points are experimental photoemission results for W (001) (1×1) (Campuzano *et al* 1981).

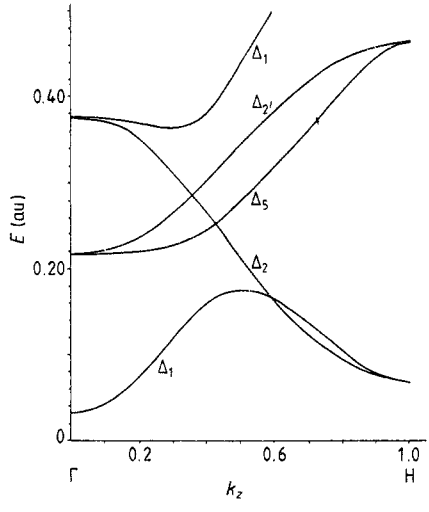

Figure 23. Bulk Mo band structure at $\boldsymbol{K} = 0$.

state was due to relativistic effects opening up band gaps between the Δ_2, $\Delta_{2'}$ and Δ_5 bands (Feder and Sturm 1975) (figure 23), but polarisation-dependent photoemission measurements have shown that it has Δ_1 symmetry, the symmetry of s, p_z and d_{z^2} orbitals and incompatible with spin–orbit states (Weng *et al* 1978). The first calculations to explain the $\bar{\Gamma}$ surface state were a self-consistent calculation (Kerker *et al* 1978), and a matching Green function calculation on Mo (001) (Inglesfield 1978b, 1979a). The surface state lies in the s–p_z/d_{z^2} hybridisation gap between the Δ_1 bands, at $E = 0.17$ au and 0.37 au in the Mo band structure shown in figure 23, and does not interact with the Δ_2, $\Delta_{2'}$ and Δ_5 bands because of its Δ_1 symmetry. As it lies well away from the Δ_1 band edges the surface state is well localised, with 60% of its charge density lying in the surface atomic cell in the Green function calculation (Inglesfield 1979a), and more than 90% in the top layer in the W (001) slab calculation (Posternak

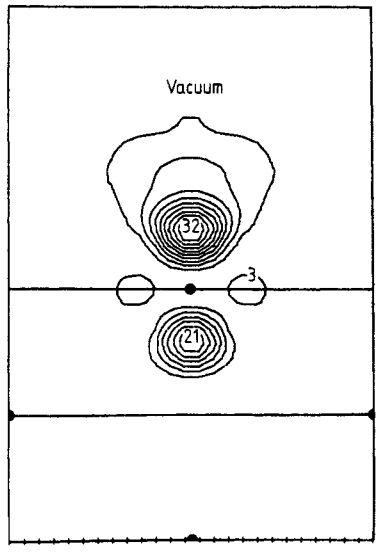

Figure 24. Contours of charge density of $d_{z^2}^2$ surface state at $\bar{\Gamma}$ on Mo (001) (Kerker *et al* 1978).

et al 1980). It is essentially a d_{z^2} *atomic-like* state (figure 24), which arises because the surface atoms do not interact very strongly with the substrate in the open BCC (001) surface. Moving away from $\bar{\Gamma}$, the calculations for both Mo and W (001) show that this surface state disperses upwards through E_F (figure 22)—it actually becomes a surface resonance away from $\boldsymbol{K} = 0$ because the symmetry restriction preventing its interaction with the bulk bands no longer applies.

The W and Mo (001) calculations show a pair of surface states/resonances which develop close to $\bar{\Gamma}$, just under E_F, and disperse upwards along the $\bar{\Gamma}\bar{M}$ direction (figure 22) (Kerker *et al* 1978, Posternak *et al* 1980). These states are made up of d_{zx} and d_{zy} orbitals, involved in bonding to the nearest neighbours in the bulk crystal, mixed in with d_{xy} and $d_{x^2-y^2}$ orbitals—in a sense they are dangling bonds (Kerker *et al* 1978). These states are particularly interesting because it has been suggested that they play a role in the phase transitions which the W and Mo (001) surfaces undergo: at about 370 K the W (001) surface goes from the (1×1) (apparently ideal) structure to a $(\sqrt{2}\times\sqrt{2})$ R45° structure (figure 2) (Debe and King 1979) (§ 6.2), and a similar phase transition takes place on Mo (001) (Felter *et al* 1977), though to an incommensurate structure. Calculations for Mo (001) showed that this pair of surface states/resonances, crossing E_F halfway along $\bar{\Gamma}\bar{M}$, have a straight Fermi line, coinciding with the new Brillouin zone boundary on the reconstructed surface (Inglesfield 1978c). The energy gap opening up along the zone boundary would then lower the energy of the occupied states, thereby stabilising the reconstruction.

The energies of the surface states and resonances on W (001) have recently been studied experimentally, using angle-resolved photoemission, over the whole of the surface Brillouin zone (figure 22) (Campuzano *et al* 1981). The results for the high-temperature (1×1) W (001) surface are in fair agreement with the calculated surface states and resonances along the $\bar{\Gamma}\bar{M}$ symmetry direction, as we can see from figure 22 (calculated for the ideal, unreconstructed surface): the states at $\bar{\Gamma}$ appear satisfactorily, and away from $\bar{\Gamma}$ a state appears to disperse upwards through E_F about halfway along $\bar{\Gamma}\bar{M}$. However, the nature of this state is controversial (Holmes and

Gustafsson 1981), and it is not clear whether it is the upper state of the calculated pair in figure 22 (with d_{zx+zy} symmetry), or the d_{z^2} state with much less dispersion than the calculation suggests. The state labelled 3 in figure 22, which has both an even and odd component, is in clear disagreement with theory.

The W (001) photoemission spectra show very interesting changes when the surface is cooled down and reconstructs (Campuzano *et al* 1980, 1981). Firstly new features appear at $\boldsymbol{K} = (\pi/a, \pi/a)$ due to umklapp from $\boldsymbol{K} = 0$ through the new surface reciprocal lattice vector $\boldsymbol{G} = (\pi/a, \pi/a)$ (figure 3): the peak at -1.4 eV is due to photoemission from bulk states at the $\Gamma_{25'}$ band edge. But more important there is evidence of a band gap opening up at the Fermi energy at $\boldsymbol{K} = (\pi/2a, \pi/2a)$ where the new Brillouin zone boundary appears. Figure 25 shows the photoemission spectra

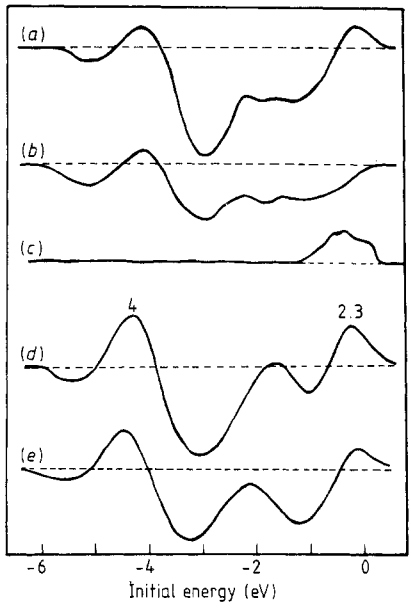

Figure 25. Difference photoemission spectra (i.e. clean−H-covered) from W (001) at $\boldsymbol{K} = (\pi/2a, \pi/2a)$, halfway along $\bar{\Gamma}\bar{M}$ symmetry line (figure 22): (*a*) (1×1) structure; (*b*) $(\sqrt{2}\times\sqrt{2})$ R45° structure; (*c*) difference spectra between clean (1×1) and clean $(\sqrt{2}\times\sqrt{2})$ R45° structures (Campuzano *et al* 1980, 1981).

in the (1×1) and $(\sqrt{2}\times\sqrt{2})$ R45° structures, and we see quite clearly that the peak due to the surface state at E_F is attenuated on reconstruction. The calculated surface density of states with $\boldsymbol{K} = (\pi/2a, \pi/2a)$ (figure 26) shows the splitting of the surface states/resonances at this point due to coupling by the $\boldsymbol{G} = (\pi/a, \pi/a)$ component of the surface potential to equivalent states at $\boldsymbol{K} = (-\pi/2a, -\pi/2a)$, and it is easy to see why this leads to a reduction in photoemission intensity. In the (1×1) phase the state at E_F has a wavefunction with a variation along the surface given by

$$\psi_{\boldsymbol{K}} \sim \exp(\mathrm{i}\boldsymbol{K}\cdot\boldsymbol{R}) \qquad \boldsymbol{K} = (\pi/2a, \pi/2a) \tag{3.10}$$

but in the $(\sqrt{2}\times\sqrt{2})$ R45° structure this couples to $\psi_{-\boldsymbol{K}}$ giving the standing waves at the new surface Brillouin zone boundary:

$$\psi_+ \sim \sqrt{2}\cos\boldsymbol{K}\cdot\boldsymbol{R} \qquad \psi_- \sim \sqrt{2}\sin\boldsymbol{K}\cdot\boldsymbol{R}. \tag{3.11}$$

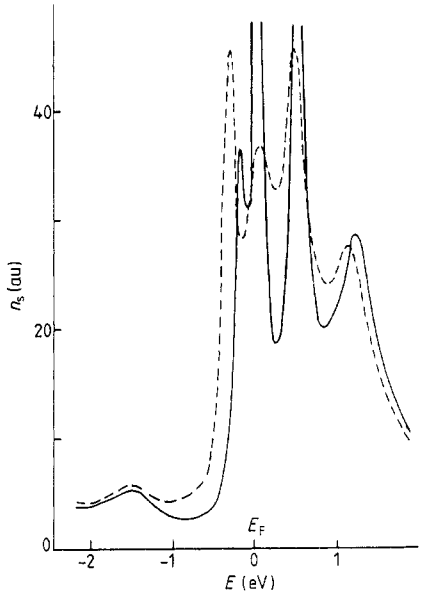

Figure 26. Surface density of states $n_{s,\boldsymbol{K}}(E)$ at $\boldsymbol{K} = (\pi/2a, \pi/2a)$ (calculated for Mo (001)). Full curve: (1×1) structure; broken curve: $(\sqrt{2} \times \sqrt{2})$ R45° structure (Campuzano *et al* 1980, 1981).

As only one of these states lies below E_F, the matrix element for photoemission into the free-electron wave with parallel component exp ($i\boldsymbol{K} \cdot \boldsymbol{R}$) is reduced by a factor of $1/\sqrt{2}$, and the emission intensity reduced on reconstruction. These results appear to support the surface-state stabilisation theory of the reconstruction (Inglesfield 1978c, Tosatti 1978). Unfortunately, when the surface state/resonance is followed in angle-resolved photoemission away from $\bar{\Gamma}\bar{M}$, the Fermi line is very curved, and the surface-state splitting can only involve a minute number of electrons (Campuzano *et al* 1981). So it seems very unlikely that the surface-state Fermi line plays any role in driving the phase transition (Inglesfield 1981), and we shall discuss other mechanisms for the surface instability in § 6.2. In the meantime we are left with unresolved discrepancies between theoretical and experimental surface-state dispersion.

3.2.3. The Ni (001) surface. The (001) surface of FCC† Ni is comparatively close-packed, and this leads to considerable differences in electronic structure from the Mo and W (001) surfaces. The surface density of states found in a self-consistent slab calculation (Arlinghaus *et al* 1980) is shown in figure 27—the band narrowing is asymmetric, because of an upward potential shift on the surface atoms (Smith *et al* 1980). In the tight-binding picture we would expect an upward shift due to d-band narrowing in the case of Ni with nine d electrons, but this cannot be the whole story as a self-consistent calculation for Cu (001) with a *full* d band gives an upward core shift of 1.5 eV (Smith *et al* 1980). Despite the band narrowing, the surface density of states is closer to the bulk on the Ni (001) surface than on the open (001) BCC surfaces of Mo and W, because each atom still has 8 out of 12 bulk nearest neighbours. This is also apparent in the surface density of states with a particular wavevector, and figure 28 gives $n_{s,\boldsymbol{K}}(E)$ at $\boldsymbol{K} = (0.1, 0.2)$ au for Ni (001) compared with the bulk density

† Face-centred cubic.

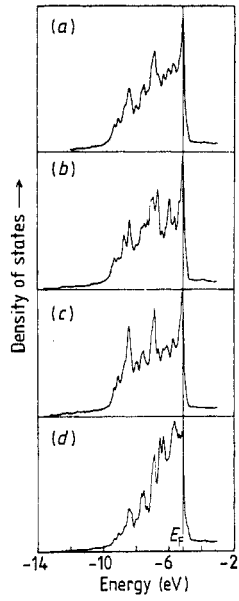

Figure 27. $n_s(E)$ for Ni (001) in nine-layer slab calculation, compared with densities of states on sub-surface layers (Arlinghaus *et al* 1980). (*a*) Total, (*b*) central plane, (*c*) second plane from surface, (*d*) surface plane.

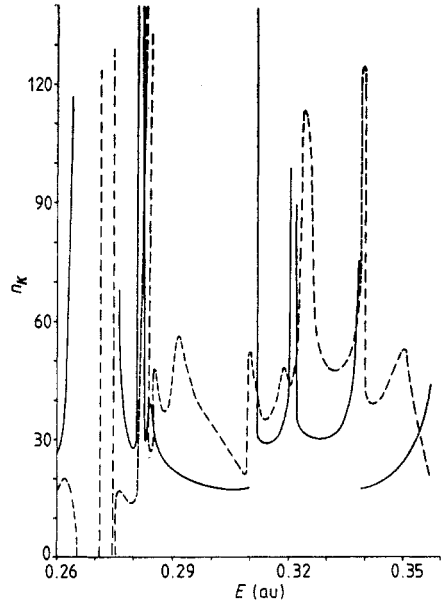

Figure 28. $n_{s,K}(E)$ (broken curve) at $\boldsymbol{K} = (0.1, 0.2)$ au for Ni (001) compared with bulk density of states at this wavevector (full curve) (non-self-consistent matching Green function calculation (Inglesfield 1978b)).

of states at this wavevector (Inglesfield 1978b). There is considerable structure in the surface density of states, with surface states and resonances, but they reflect band edge singularities in the bulk density of states. This figure shows the effect we described in the introduction to this section—the reduction in weight at the band edges close to $E = 0.27$ au, due to the presence of the surface states.

The Ni (001) charge density (figure 29) shows greater smoothing than the W (001) charge density (figure 21), as we would expect with its closer packing. The smoothing involves the s–p free-electron density which extends further into the vacuum than the d-electron density—this remains spherical at the surface as in the bulk with none of the bonding effects we see in figure 21. Once again the calculated work function is in excellent agreement with experiment: $\varphi = 5.1$ eV (Arlinghaus *et al* 1980) compared with experimental values of 5.0–5.2 eV. It is remarkable that all the work functions which we have discussed are so similar, on surfaces with widely differing electron density, and we shall discuss the reasons for this in § 4.

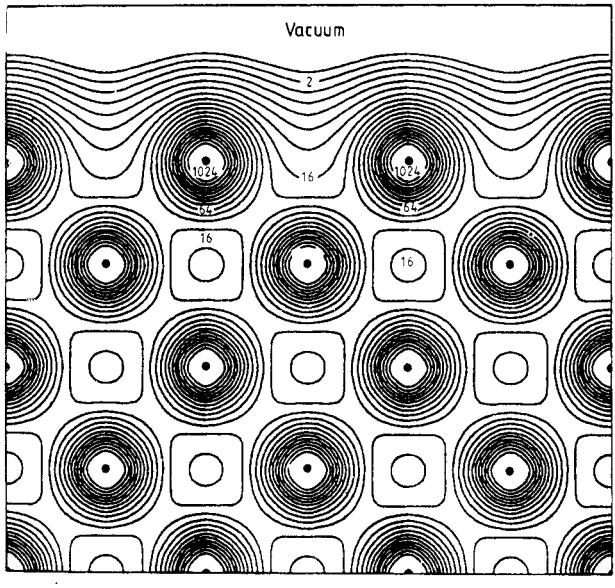

Figure 29. Contours of charge density at Ni (001) surface (Arlinghaus *et al* 1980).

The Ni (001) surface (and similarly Cu (001)) shows some characteristic surface states. The first surface state predicted for a transition or noble metal was for Cu (001) in the s–p/d hybridisation gap, between the Δ_1 bands in the ΓX direction (cf the bulk Ni band structure, figure 19) (Gurman and Pendry 1973). Gurman and Pendry found a surface state near the bottom of the gap, with a decay length of about 10 au; this is unlike the W (001) atomic-like hybridisation gap state (§ 3.2.2), and as it can be derived from a generalisation of the two-band model (2.21)–(2.27) (Pendry and Gurman 1975) it is more like a Shockley state. The self-consistent slab calculation shows an s–p/d hybridisation gap surface state on Ni (001), at about −9.3 eV around $\bar{\Gamma}$ (figure 30), but it has not yet been identified experimentally. Many other surface states and resonances occur close to the band edges, but particularly interesting is a surface state above the top of the d bands at $\bar{M}$ (figure 30). This is a Tamm state, pulled off the top of the d bands by the shift in surface potential. At $\bar{M}$, the projected band structure is in the XW direction in the bulk Brillouin zone, and the topmost d band is a very flat band (figure 19) made up of d_{xy} orbitals—these hardly interact in the ⟨001⟩ direction, so it is very easy to pull a localised state from them by a small shift in the potential at the surface.

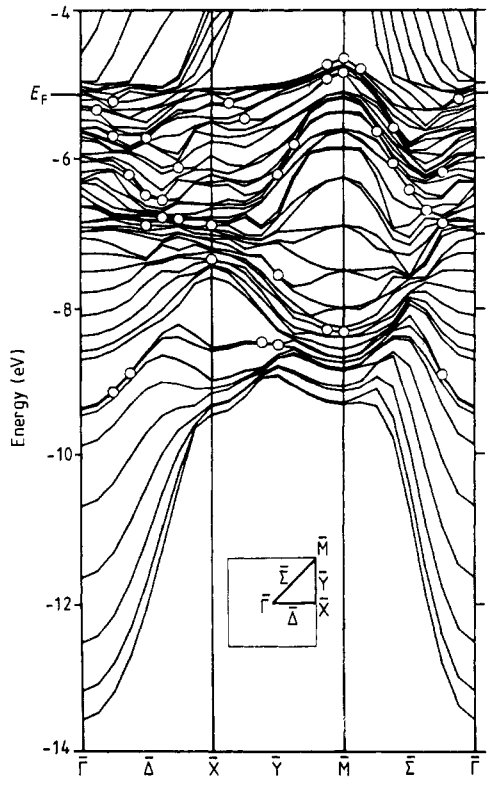

Figure 30. Energies of states in Ni (001) slab as a function of $\boldsymbol{K}$. Circles indicate surface states/resonances (Arlinghaus *et al* 1980).

In the *paramagnetic* results for Ni (001) given in figure 30 this Tamm state lies about 0.5 eV above the Fermi energy. However, Plummer and Eberhardt (1979) have found an apparent surface state just below E_F, using angle-resolved photoemission, which has polarisation dependence consistent with d_{xy} orbitals. Now Ni is ferromagnetic because the electrons with majority spin feel a more attractive potential than those with minority spin, and the effect of this is to pull the majority spin XW band below E_F (Wang and Callaway 1977); so the observed surface state is probably a majority spin Tamm state (Plummer and Eberhardt 1979). A spin-polarised self-consistent calculation by Wang and Freeman (1980) confirms that the majority spin Tamm state lies just below E_F along most of the $\bar{Y}$ line in the surface Brillouin zone, but unfortunately just above at $\bar{M}$ where it is still seen experimentally. The equivalent Tamm state has been observed on Cu (001) in angle-resolved photoemission, lying 1.8 eV below E_F (Heimann *et al* 1979).

The band structure of FCC transition metals shows a band gap in the free-electron s–p band, well above E_F in the ⟨001⟩ direction (ΓX). However, E_F lies in this band gap in the noble metals in the ⟨111⟩ direction (ΓL), and the corresponding Shockley surface state has been seen 0.4 eV below E_F in normal photoemission from Cu (111) (Gartland and Slagsvold 1975). The same state has been predicted to occur on Ni (111) about 0.5 eV above E_F (Larsson and Nilsson 1981), where it should be observable using inverse photoemission (§ 3.1.2).

3.2.4. Surface magnetism. The change in electronic structure at the surface of transition metals suggests that possible changes in magnetic properties should be looked for. Recently spin-polarised photoemission experiments have been carried out on Ni, and photoemission calculations reproduce the experimental results with a spin splitting of the d levels of 0.33 eV, without any change in magnetism at the surface (Moore and Pendry 1978). As surface states have been observed on the Ni (110) surface split by the same amount (Eberhardt *et al* 1980) (within experimental error), this suggests little change in magnetism at the surface of Ni—a consequence of the surface density of states being similar to the bulk density of states. The magnetism can, in fact, be calculated self-consistently using the local spin-density approximation in which spin-up and spin-down electrons feel different exchange-correlation potentials (von Barth and Hedin 1972). Using this approach Wang and Freeman (1980) find that the surface atoms on Ni (001) do indeed remain magnetic, though with a magnetic moment reduced by about 20% compared with the bulk. A contributory factor to this reduction is the Tamm state at $\bar{M}$ being split off *above* E_F in their calculation (§ 3.2.3).

As well as the possibility of reduced magnetism on the surface of a ferromagnet, there is also the possibility of a ferromagnetic surface layer on a bulk paramagnet (Edwards 1979)—for example, the big peak in the surface density of states on the (001) surface of a BCC metal (§ 3.2.1) might lead to a ferromagnetic instability if it coincides with E_F. V, with a nearly half-filled d band and a BCC structure, is a possible candidate, and experiments on the temperature dependence of the magnetic susceptibility indicate a radius-dependent Curie–Weiss behaviour, coming perhaps from surface ferromagnetism, as well as the bulk Pauli susceptibility (Akoh and Tasaki 1978).

3.2.5. Surface states on transition metals: conclusions. We have just seen that the surface states on Ni (001) may play a role in surface magnetism, involving as it does very small changes in the density of states at E_F. The question remains—what role do they play in bonding at surfaces? Surface states and resonances from a large part of the surface Brillouin zone contribute to the peak in $n_s(E)$ at the Fermi energy on W (001) and Mo (001), and we suggest in § 6.2 that this peak leads to the instability of the ideal surface—hence the surface phase transitions. However, the evidence from angle-resolved photoemission is that *individual* surface states play no part in driving the phase transition, through the Fermi surface instability mechanism (§ 3.2.2). Surface states are, of course, sensitive to adsorbed atoms, and their removal by H adsorption is one way of recognising them in photoemission experiments. However, this does not mean that individual surface states intrinsic to the clean metal surface play a part in the bonding of chemisorbed atoms. Clearly an adatom approaching an ideal surface destroys the $\boldsymbol{K}$ conservation and once again it is the total surface density of states, rather than individual surface states, which is more relevant. (The situation is rather different on semiconductor surfaces, as we shall see in § 3.3, where surface states over the whole surface Brillouin zone are equivalent to dangling chemical bonds.)

The importance of surface states lies chiefly in the way that they illustrate particular effects in surface electronic structure: the atomic-like states at $\bar{\Gamma}$ on W and Mo (001) are a result of the open geometry of the surface, other states on these surfaces have some of the properties of dangling bonds, and the Tamm states on Ni (001) come from the change in surface potential, for example.

3.3. *Surfaces of semiconductors*

3.3.1. Chemical bonding and surface states. The surfaces of semiconductors provide an interface between detailed calculations of surface wavefunctions and simple chemical bonding ideas. The bulk energy bands of Ge and Si can be unfolded into an extended zone scheme and are then recognisably distortions of free-electron bands, though with a large energy gap on the Jones zone boundary (Heine and Jones 1969). From this point of view the electronic structure can be thought of as free-electron-like, perturbed by the (rather strong) ionic pseudopotentials; this scheme may even be applied to diamond (Phillips 1968). On the other hand, in the chemical bonding picture the group IV semiconductors and diamond are held together by local sp^3 bonds—the local description should improve as the band gap increases. The two pictures are, of course, related, and a full calculation of bulk electronic structure based on band theory produces a piling up of bond charge between atoms (Heine and Jones 1969).

The chemical bonding picture explains the general features of the surface electronic structure of the group IV semiconductors (García-Moliner and Flores 1976). When a Ge, Si or diamond (111) surface is made, one sp^3 bond directed perpendicular to the surface is cut on each atom. Linear combinations of these dangling orbitals give surface states with definite $\boldsymbol{K}$, with energy in the band gap between occupied and unoccupied states, so we obtain one band of surface states on the ideal (111) surface. Similarly on the (110) surface there are two atoms per surface unit cell, and as one bond is cut per atom there should be two bands of surface states; finally on the (001) surface, two bonds are cut on the one atom per surface unit cell, again giving two bands of surface states. Full calculations of the electronic structure confirm that this simple picture is essentially correct, and using the wavefunction matching method (§ 2.1.1) Appelbaum and Hamann (1973) obtained the surface-state charge density for the Si (111) (1×1) surface shown in figure 31, with clear dangling bond character.

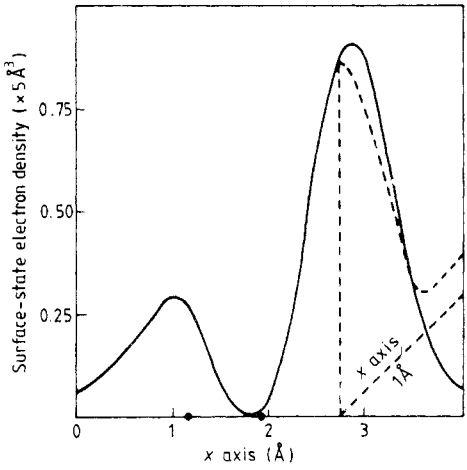

Figure 31. Electron density in the dangling bond surface state on Si (111). The dots mark atomic planes and the broken curve shows the variation parallel to the surface (Appelbaum and Hamann 1973).

A simple connection can be made between the chemical bond picture and full calculations by using a two-band model to describe the bulk electronic structure with an *effective* pseudopotential matrix element giving the band gap (Jones 1972, Yndurain

and Elices 1972). The states at the bottom of the gap are bonding states, so the Shockley condition (negative V_g) is satisfied (§§ 2.2 and 3.1.1) and a surface state occurs. This is well localised because the band gap is large.

The dangling bond surface states contain one unpaired electron per bond, but electron paramagnetic resonance experiments show far fewer unpaired electrons than this, with one free spin for every 10 or so surface atoms on Si (111) (Haneman 1968), and even fewer on Ge (Higinbotham and Haneman 1973). The reason for this is that the ideal surfaces are unstable, and the Si, Ge and diamond surfaces reconstruct (Marsh and Farnsworth 1964, Haneman 1975) so that the electrons in the dangling bonds pair up. We shall discuss the surface reconstructions and relaxations in greater detail in subsequent sections, and shall see that they introduce *back-bonding* surface states in addition to the dangling bonds. The freshly prepared surface of silica also contains dangling bonds, probably sp^3 orbitals on surface Si, largely removed by reconstruction and interaction with adsorbed species (Hochstrasser and Antonini 1972).

3.3.2. Charge neutrality at semiconductor surfaces. From a chemical bonding point of view we would expect dangling bond surface states on an ideal, unreconstructed surface to lie at E_F so that they are half-filled: this turns out to be true when the surface electronic structure is considered in detail. In the simple one-dimensional case, we can see from figure 9 that half a state (equivalent to one electron) is lost in the valence band when a surface state occurs. So in order to maintain overall charge neutrality the surface potential must adjust itself self-consistently till the surface state lies precisely at E_F and is half-filled (García-Moliner and Flores 1976). The bulk material is automatically neutral, as the changes in charge density are localised at the surface, and positioning the surface state at E_F leads to surface neutrality. The full three-dimensional case is more complicated, but it can be rigorously proved that the bulk is neutral (at least for (001), (110) and (111) surfaces of homopolar semiconductors) (Kleinman 1975a, b). States are still removed from the valence band, in particular $\frac{1}{4}$ state at each band edge (Inglesfield 1978a); the changes in $\sigma(r, E)$ remain localised at the surface, and the partial occupancy of surface states ensures surface neutrality, and hence overall neutrality. The surfaces need not be neutral, however, in the case of zincblende compound semiconductors like GaAs, in which the (111) surfaces consist ideally of either Ga or As atoms. In this case the surface states position themselves relative to E_F so that the Ga (111) surface is positively charged and the As $(\bar{1}\bar{1}\bar{1})$ surface is negatively charged (Chadi and Cohen 1975).

The self-consistent positioning of the partially filled surface-state band in the middle of the band gap is important in Fermi level pinning at surfaces and interfaces of doped semiconductors (Many *et al* 1971).

3.3.3. The Si (111) surface. The (111) surface of cleaved Si reconstructs to form a metastable (2×1) structure, which on annealing forms the stable (7×7) structure (Mönch 1979). Various models for the (2×1) structure have been proposed including the Haneman model (Haneman 1961), in which alternate rows of surface atoms are raised and lowered, doubling the size of the real space unit cell. This model has received strong support from a very useful energy minimisation calculation carried out by Chadi (1978) (§ 6.3), who finds that the (111) surface energy is minimised with vertical displacements of the surface atoms of +0.59 au and −0.83 au, together with lateral displacements in the second layer of atoms which keep the bond lengths

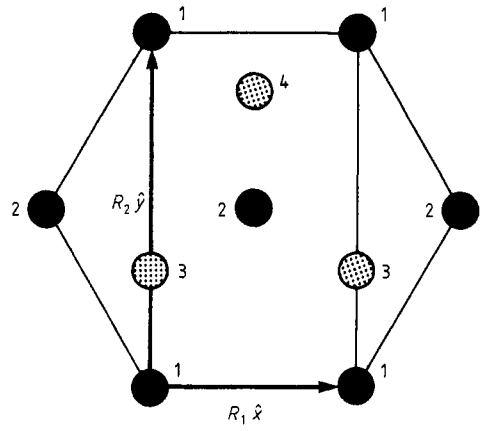

Figure 32. Unit cell for (2×1) reconstruction of Si (111). Atoms 1 move out of the surface, atoms 2 move in and atoms 3, 4 in the sub-surface layer undergo lateral displacements to keep bond lengths approximately constant (Chadi 1978).

between the surface and substrate nearly constant (figure 32). Recent LEED experiments are in agreement with a buckled surface structure, though with less buckling than Chadi's theoretical estimate (Feder *et al* 1979). Further support for the buckled surface comes from measurements of the binding energy of the Si 2p level, using x-ray photoemission—these experiments show shifts to higher and lower binding energies than in the bulk, consistent with surface atoms moving up and down (Brennan *et al* 1980).

Several calculations have been carried out on the electronic structure of the reconstructed surface. A self-consistent slab calculation was performed by Schlüter *et al* (1975) in which surface atoms were raised and lowered by 0.34 au and −0.21 au, respectively, again with lateral shifts in the substrate layer. The (2×1) reconstruction halves the size of the surface Brillouin zone, splitting the dangling bond surface state, and in this calculation opening up a band gap of about 0.27 eV between the occupied and unoccupied states (figure 33). In chemical bonding terms, the change in bond

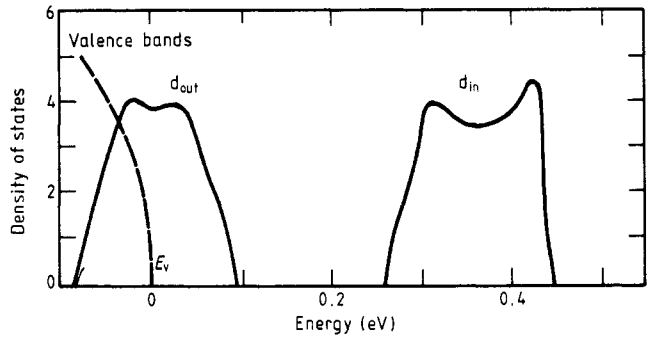

Figure 33. $n_s(E)$ for the Si (111) reconstruction showing splitting of the dangling bond surface states. E_v is the bulk valence band edge (Schlüter *et al* 1975).

angle on reconstruction changes the hybridisation, and the dangling bond on the lowered atom has more p_z character, consequently being raised above the Fermi energy, whereas the raised atom has more s character and drops in energy. Electronic charge (about 0.3 *e*) (Chadi *et al* 1980) is transferred from the lowered atoms to the

raised atoms, giving a surface with some ionic character; the reduction in energy of the occupied states stabilises the reconstruction. In addition to the dangling bonds, Schlüter *et al* (1975) find surface states. 0.5 eV below the valence band edge at $\bar{\Gamma}$, dispersing down to −3.5 eV at the zone edge, associated with back bonds between the surface atoms and the substrate. Other back-bonding states occur deeper down in the valence band.

Experimental results confirm that a band gap opens up in the surface states, optical absorption measurements suggesting a direct gap of 0.26 eV (Chiarotti *et al* 1971), in good agreement with the calculation of Schlüter *et al* (1975). Photoemission experiments also show a gap at E_F, and a peak at about −0.8 eV in normal emission attributed to the dangling bond surface state (Parke *et al* 1980), though this might also have a back-bonding surface-state component (Schlüter *et al* 1975). The deeper-lying back bonds also show up in the photoemission experiments, in fair agreement with theory (Parke *et al* 1980).

The actual structure of the (7×7) form of Si (111) is not known for certain, and several suggestions have been made including a regular array of surface vacancies (Lander and Morrison 1963) or adatoms (Harrison 1976), and periodic lattice displacements (Tosatti and Anderson 1974). A full analysis of the LEED results has not been carried out for this structure, with its large surface unit cell, but a kinematic analysis casts doubt on the vacancy and adatom models (Miller and Haneman 1979). The reconstruction opens up a gap in the surface-state bands, but there is doubt about the density of states at E_F, which is clearly related to the extent of the free surface-state Fermi line: some photoemission results suggested that the emission from the dangling bonds is finite at E_F (Rowe *et al* 1975), whereas recent work shows a very low density of surface states at E_F, and a dangling bond peak at −0.8 eV as in the (2×1) reconstruction (Chadi *et al* 1980, Hansson *et al* 1980). On the basis of atom scattering experiments it has now been suggested that the (7×7) reconstruction has a completely different structure from previous notions—a regular array of large, double-layer islands (Cardillo 1981). Support for this has come from LEED experiments on H-covered (7×7) Si (111) which has a much simpler LEED pattern than the clean (7×7) surface, compatible with the island structure (McRae and Caldwell 1981) (figure 34). McRae and Caldwell suggest that on the clean (7×7) surface the dangling bonds cause a

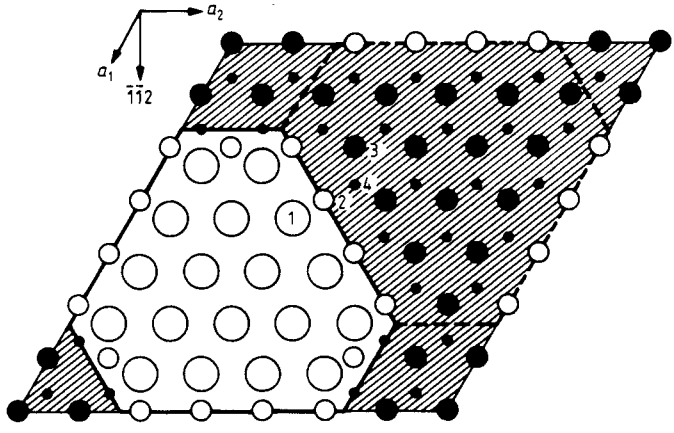

Figure 34. Model of Si (111) (7×7) reconstruction, with islands and troughs indicated by open and shaded areas (McRae and Caldwell 1981).

buckling *within* these islands and troughs, which is removed by H adsorption to give a much simpler LEED pattern. The removal of the buckling is analogous to the reversion of the Si (111) (2×1) structure to a (1×1) structure on H adsorption (Ibach and Rowe 1974), due to saturation of the dangling bonds by Si–H bond formation. This local buckling can clearly explain the resemblance of the (7×7) photoemission spectrum to the (2×1).

3.3.4. The Si (001) surface. The dangling bonds on the (001) surface of Si cause it to reconstruct to a (2×1) structure also (Mönch 1979), and Chadi (1979a) has found that the energy is minimised if the surface atoms move together to form asymmetric dimers (figure 35). The atomic displacements obtained in the energy minimisation method (§ 6.3) are vertical and lateral shifts of +0.08 au and +0.87 au for atoms of type 1, and shifts of −0.82 au and −2.04 au for atoms of type 1′ (figure 35), with

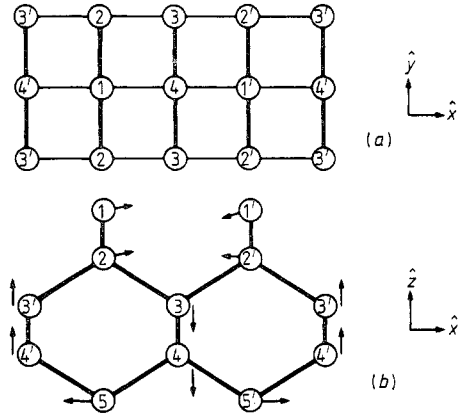

Figure 35. Si (001) (2×1) reconstruction: (*a*) top view; (*b*) side view (Chadi 1979a).

smaller displacements extending five layers into the solid. A LEED analysis had already shown that a symmetric dimerisation model gave quite good agreement with experiment (Jona *et al* 1979), but this model gives overlapping surface-state bands with a finite density of states at E_F (Ihm *et al* 1980), in disagreement with photoemission results (Himpsel and Eastman 1979). The asymmetric dimer structure, on the other hand, gives a band gap in the dangling bond surface states with zero density of states at E_F (Chadi 1979a).

In the unreconstructed surface the two dangling bonds per surface atom give rise to two bands of surface states in the band gap (Appelbaum *et al* 1975). The surface states and resonances in the (2×1) reconstruction (Ihm *et al* 1980) are shown in figure 36, calculated with the self-consistent pseudopotential slab method (§ 2.3.3), and we see that there are still two bands of surface states in the energy gap, even though the surface Brillouin zone is halved in size. There are two linear combinations of the four dangling bonds per surface unit cell (doubled in size in the reconstructed surface), the other two combinations giving states mixed in to the valence and conduction bands (Appelbaum *et al* 1975). Figure 36 shows that the band gap surface states are pushed apart in the asymmetric dimer structure compared with the symmetric dimer, giving the zero density of states at E_F as observed. Other states shown in figure 36, at −10.4 eV and −4 eV at $\bar{K}$ for example, are back-bonding states and states localised on sub-surface atoms.

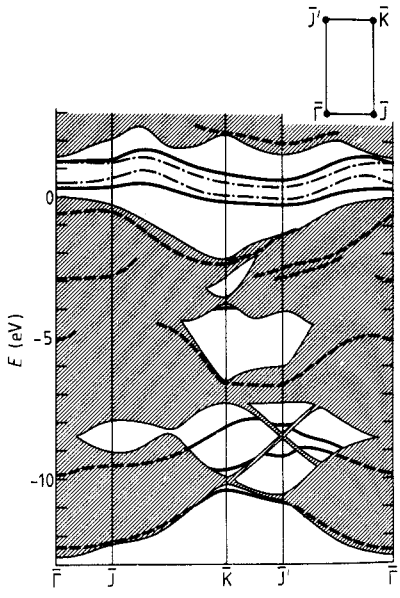

Figure 36. Surface states and resonances in Si (001) asymmetric dimer (2×1) reconstruction, as a function of $\boldsymbol{K}$ in surface Brillouin zone. The shaded area shows the projected bulk Si bands. The chain curve shows surface states for a symmetric dimer reconstruction (Ihm *et al* 1980).

The total charge density in this reconstructed surface is given in figure 37—the charge density is bulk-like beyond the second layer, with very clear piling up of bonding charge between atoms. In the top layer the reconstruction leads to an asymmetric covalent bond between the atoms in the dimer, with charge transferred from the lowered atom to the raised atom. The charge transfer comes about because the band gap surface state with lower energy has charge concentrated on the raised atom (Ihm *et al* 1980), as in the (2×1) Si (111) surface reconstruction.

3.3.5. Surfaces of compound semiconductors. The bulk bonding in compound semiconductors is intermediate between covalent and ionic, and this leads to new types of surface states. We shall concentrate on the III–V and II–VI compounds which crystallise in the zincblende structure, such as GaAs, ZnSe, etc, with cations and anions arranged alternately on a diamond lattice. To discuss the bulk electronic structure in band structure terms, it is convenient to write the total pseudopotential, a superposition of potentials v_M on the cations and v_X on the anions, in terms of the average potential:

$$\bar{v} = \tfrac{1}{2}(v_M + v_X) \tag{3.12}$$

and a difference potential (Cohen and Heine 1970):

$$\Delta v = \tfrac{1}{2}(v_M - v_X). \tag{3.13}$$

The average potential in GaAs and ZnSe, for example, is close to the Ge pseudopotential (Ge is in between Ga and As in the periodic table), whereas the difference potential increases in going from GaAs to ZnSe, associated with the increase in electronegativity difference. The band structures of GaAs and ZnSe are basically similar to that of Ge, with four valence bands separated by a band gap from the conduction bands (figure 38). However, in the case of the compounds, Δv contributes to the main band

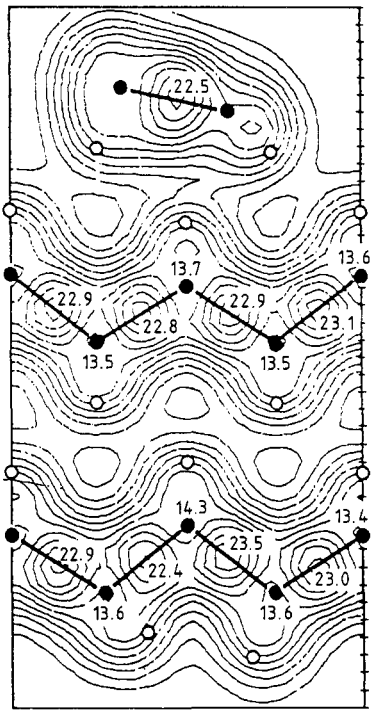

Figure 37. Contours of charge density at (2×1) reconstructed Si (001) surface (Ihm *et al* 1980).

gap in addition to $\bar{v}$: as the pseudopotential matrix elements are large it is necessary to go beyond lowest-order perturbation theory, and the band gap (on the (110) Jones zone faces) is given in terms of the effective matrix element V_{eff} (220) (Heine and Jones 1969):

$$E_{\text{gap}} = 2|V_{\text{eff}}(220)|$$

$$V_{\text{eff}}(220) = \bar{v}(220) + \frac{\bar{v}(111)^2 + \Delta v(111)^2}{E_{110} - E_{001}}. \tag{3.14}$$

We see that the $\boldsymbol{g} = 2\pi/a$ (1, 1, 1) component of the total pseudopotential contributes to the gap—in fact, it dominates V_{eff}—and this contains the *ionic* part of the pseudopotential Δv, as well as the covalent part $\bar{v}$. The other main effect of Δv is to open up a band gap between the lowest valence band and the upper three (figure 38) (Cohen and Heine 1970).

We can understand the bulk electronic structure in an alternative way by starting at the other extreme—a completely ionic model of the electronic structure, in which electrons are transferred from the cations to the anions to fill the s and p orbitals in the valence shell. The four valence bands correspond to these occupied anion states, the split-off low-lying band corresponding to the s level. As the lowest excitation in an ionic molecule like $M^{2+}X^{2-}$ corresponds to transferring an electron from the anion to the cation, we expect the conduction bands to correspond to states localised on the cations (though in reality they spread out onto the anions as well).

The zincblende compounds cleave on the (110) face, which is heteropolar with one atom of each type per surface unit cell. Figure 39 shows the surface density of

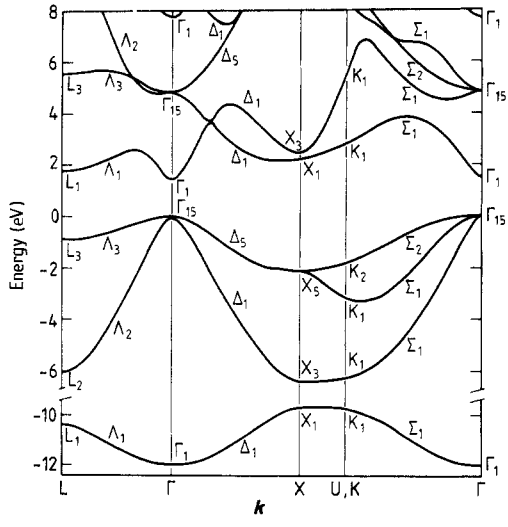

Figure 38. Band structure of GaAs (Cohen and Heine 1970).

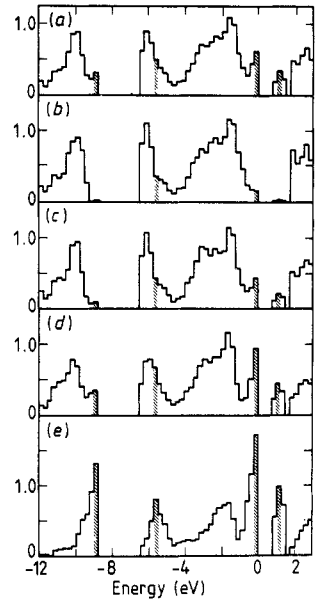

Figure 39. $n_s(E)$ for ideal GaAs (110) and densities of states on sub-surface layers. Shaded blocks represent surface states, and the energy zero is at the valence band edge (Chelikowsky and Cohen 1976). (*a*) Total, (*b*) layer 5, (*c*) layer 3, (*d*) layer 2, (*e*) surface.

states for GaAs (110), calculated using the self-consistent pseudopotential slab method (Chelikowsky and Cohen 1976) (§ 2.3.3), and we see that there are two bands of surface states associated with the main band gap, with states right at the valence band edge strongly localised on the surface As atoms, and those under the conduction band edge concentrated on the Ga. These surface states develop from the two bands of dangling bond states on the (110) surface of the elemental semiconductor: Δv splits the bands further, and removes the degeneracy along $\bar{X}\bar{M}$ in the surface Brillouin zone (figure 40). In the ionic limit (more appropriate to ZnSe than GaAs), the surface

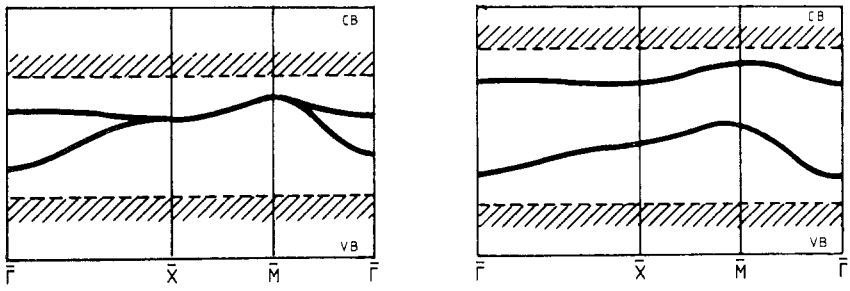

Figure 40. (110) surface state bands in homopolar semiconductors (upper panel) are split by Δv in compound semiconductors (lower panel) (García-Moliner and Flores 1976).

states split off the bulk bands because of the different Madelung potential at the surface (Levine and Mark 1966). The removal of neighbouring ions by the surface reduces the Madelung potential, raising the energy of an electron on an anion and lowering it on a cation. This produces states above the top of the valence band which are strongly localised on the anions, and similarly surface states below the conduction band which tend to be localised on the cations. The lower band of surface states lies below E_F and is occupied; as in the case of elemental semiconductors, this cancels the loss of states in the valence band and at the band edge, to give overall charge neutrality.

As well as these states in the main band gap, surface states occur at the top of the lowest band (figure 39), which are well-localised in s orbitals on the surface As atoms. As we would expect from the ionic model of the electronic structure, this lowest band is itself concentrated on the As atoms, and it is the change in electrostatic potential at the surface which pulls off this band of surface states. Besides these states, there are also back-bonding states with energies in the valence band, as in the case of Si.

The surface states shown in figure 39 are not in agreement with experiment: angle-resolved photoemission from GaAs (110) shows a band of surface states about 1 eV below the valence band maximum (Knapp and Lapeyre 1976, Huijser *et al* 1978), lower than the calculation on the unrelaxed surface would indicate for the dangling bond/ionic states localised on the As atoms. Moreover, the absence of Fermi level pinning in the doped semiconductor shows that there are no unoccupied surface states in the band gap (Gudat and Eastman 1976), so the states localised on the Ga atoms shown in figure 39 must lie above the conduction band minimum. In fact, experiments indicate that there are no surface states in the optical band gap on the (110) surfaces of InAs, GaSb and GaAs, and only on GaP (110) are there empty surface states below the conduction band minimum (Huijser *et al* 1977). The reason for the absence of surface states is that the surface reconstructs, and analysis of the LEED data suggests that the As atoms move out of the surface and the Ga atoms move in, rather like the Si (111) reconstruction: a calculation by Chadi (1979b) shows that the energy is minimised when the angle of the nearest-neighbour cation–anion axis is rotated by 27° from the surface plane, in good agreement with the LEED results (Tong *et al* 1978). When the reconstruction (actually a *relaxation* because the surface unit cell stays the same) is included, the As-localised dangling bond/ionic states are pushed down to about 0.6 eV below the valence band maximum, and the Ga-localised states are pushed above the conduction band minimum (Chelikowsky and Cohen 1979) (figure 41).

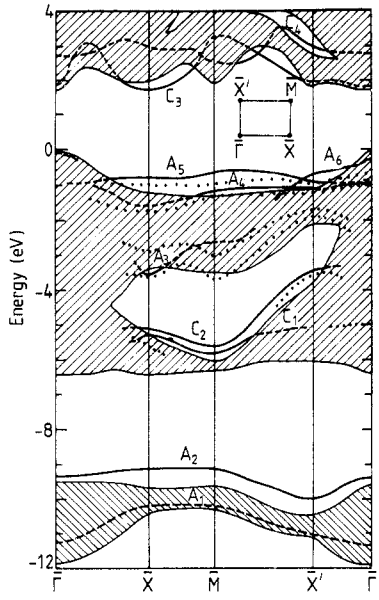

Figure 41. Surface states and resonances on relaxed GaAs (110) as a function of $\boldsymbol{K}$ in surface Brillouin zone. The shaded area shows the projected bulk GaAs bands. The full curves show the calculated results (Chelikowsky and Cohen 1979) and the dotted curves experimental results (Huijser *et al* 1978).

4. Work functions

The work function φ provides an important test of a self-consistent surface potential, and the calculations which we have reviewed in the last section give values in good agreement with experiment. It is also inherently interesting, as it reflects changes in the charge distribution at the surface, and we shall now study it in more detail. A surprising property of φ is that it varies remarkably little in going from element to element (Rivière 1969, Nieminen and Hodges 1976); for instance, the work functions of s–p bonded metals vary between 2 eV for Cs and 4 eV for Al, whereas the electron density varies by a factor of 20 in going from Cs to Al. For the transition metals φ tends to lie between 4 and 5 eV, and in the semiconductors Ge and Si it is also about 4 eV. φ can be divided into two contributions (Seitz 1940, Lang and Kohn 1971)—the potential barrier D set up by the redistribution of charge at the surface, and the absolute Fermi energy $\bar{\mu}$ of the electrons in the absence of such a surface dipole:

$$\varphi = D - \bar{\mu}. \tag{4.1}$$

The reason why the work function is so constant is that a large electron density, which leads to a high value of $\bar{\mu}$ because of the high Fermi energy, also gives a large surface dipole D. Because of the dipole contribution, φ varies somewhat from surface to surface, and experimental examples of this are:

FCC Al (Grepstad *et al* 1976)

(111) 4.24 eV (100) 4.41 eV (110) 4.28 eV

FCC Cu (Gartland *et al* 1972)

(111) 4.94 eV (100) 4.59 eV (110) 4.48 eV

BCC W (Strayer *et al* 1973)

(110) 5.25 eV (100) 4.63 eV (111) 4.47 eV.

The surfaces are listed in order of decreasing atomic density, and we see that there is a tendency for the planes of greatest density to have the largest work functions, though Al (111) is an exception to this.

Before we can discuss the separate contributions to φ, we must consider what we mean by the *redistribution* of charge at the surface, defining the system without a surface dipole. One convenient choice of reference distribution is to use the bulk charge distribution right up to the boundaries of undistorted Wigner–Seitz cells at the surface (Nieminen and Hodges 1976) (figure 42): $\bar{\mu}$ is the absolute Fermi energy

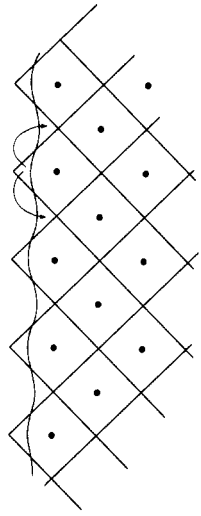

Figure 42. Schematic bulk Wigner–Seitz cells continued up to the surface. Arrows and wavy line indicate charge redistribution at the surface.

within this system measured from the vacuum zero, and D is the dipole potential produced by the deviations of the actual, self-consistent charge density from this reference distribution. If the solid is close-packed, the Wigner–Seitz cells are fairly spherical, and being neutral each cell produces zero electric field—so the potential in the interstitial region between cells is zero in the reference system. This means that in the real crystal with redistribution of surface charge, $\bar{\mu}$ is E_F measured from the interstitial potential, and $(-D)$ is the value of this interstitial potential with respect to the vacuum zero.

Using this reference distribution, Heine and Hodges (1972) have estimated $\bar{\mu}$ from bulk cohesive properties and then calculated D from measured work functions (table 1). We see that $\bar{\mu}$ makes the biggest contribution to the work function in the low-density elements like the alkalis, whereas D dominates at high density. The tendency of D and $\bar{\mu}$ to compensate for each other also seems to be at work in the d-bonded transition metals: in the case of Ag Nieminen and Hodges (1976) estimate that $\bar{\mu}$ is -1.4 eV and D is 2.6 eV, giving a (polycrystalline) work function of 4.0 eV;

Table 1. Contributions to work functions of simple metals (Heine and Hodges 1972). φ is the work function for polycrystalline materials in this table.

	r_s (au)	D (eV)	$\bar{\mu}$ (eV)	φ (eV)
Al	2.07	3.4	−0.8	4.2
Zn	2.30	2.9	−1.4	4.3
Mg	2.65	2.0	−1.7	3.7
Ca	3.27	1.1	−1.6	2.7
Na	3.93	0.7	−2.0	2.7
K	4.86	0.2	−2.2	2.4
Cs	5.63	—	(−2.2)	2.1

on the other hand, in W $\bar{\mu}$ is much higher, +1.4 eV, but D is also higher, 6.0 eV, giving a work function of 4.6 eV. There is really an efficient feedback mechanism at work—if $\bar{\mu}$ increases, the electrons tend to penetrate further into the vacuum, but this sets up a surface dipole to increase the work function and bring down the penetration length of the electrons (Heine and Hodges 1972). It is not surprising that the work functions of Ge and Si should be in the same range as metal work functions, as we saw in § 3.3 that their electronic structure can be obtained by treating the pseudopotential as a perturbation on a free-electron gas, and apart from the relatively small bonding charge, the charge density is not greatly affected.

The large surface dipoles listed in table 1 are a consequence of the reference surface charge distribution being unrealistic. It is often a good approximation for the charge distribution and potential in a solid to superpose the free-atom values, and we can use this as our reference system for which D is defined to be zero. The change from this charge distribution at the actual surface should then be quite small, giving smaller values of D and work functions which are closer to $-\bar{\mu}$. As an example of this, Nieminen and Hodges (1976) discuss Au for which a superposition of free atoms gives an electrostatic potential in the interstitial region between atoms of −4.4 eV compared with 0 for the Wigner–Seitz reference system. With respect to the latter system they estimate that D is 3.6 eV, so the surface dipole is only −0.8 eV with respect to a superposition of free atoms. This corresponds to a very small shift of the electrons from the free-atom charge distribution.

4.1. Work function variation and surface smoothing

The tendency for densely packed surfaces of a particular crystal to have larger work functions shows that they have the largest surface dipoles with respect to the Wigner–Seitz and atomic charge reference distributions (both of which give an internal contribution to the work function independent of crystal surface). The reason for this is that the smoothing of the surface charge density, which we encountered in § 3 (figures 12 and 29), transfers charge to the hollows between atoms on open surfaces (figure 42), setting up a negative dipole which reduces φ (Smoluchowski 1941). This smoothing is by no means complete, however, and the planar averaged charge density $\rho_0(z)$, calculated for different surfaces of FCC Al by a variational method (Monnier and Perdew 1978), still falls off less abruptly on the open (110) surface than on the close-packed (111) surface (figure 43), as we would expect from the atomic charge distribution.

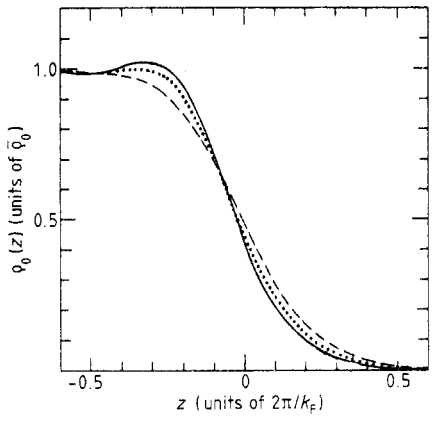

Figure 43. Planar averaged charge density at different Al surfaces (Monnier and Perdew 1978). ——, (111); · · · · ·, (001); – – –, (110).

4.2. Jellium calculation of work functions

The work functions of s–p bonded metals can be found from the self-consistent jellium calculations of Lang and Kohn (1970, 1971), in which the ions are smeared out into a uniform positive background cut off sharply at the surface (§ 3.1). In this model there is no difficulty with the reference charge distribution, D being the rise in electrostatic potential across the surface due to charge overflow, and $\bar{\mu}$ the Fermi energy measured from the bulk electrostatic potential:

$$\bar{\mu} = \tfrac{1}{2}k_F^2 + \bar{V}_{xc}. \tag{4.2}$$

The results for φ found using Lang and Kohn's jellium charge densities are shown in figure 44, and we see that they are in good agreement with experimental values for polycrystalline materials. In particular they reproduce the observed trend that the

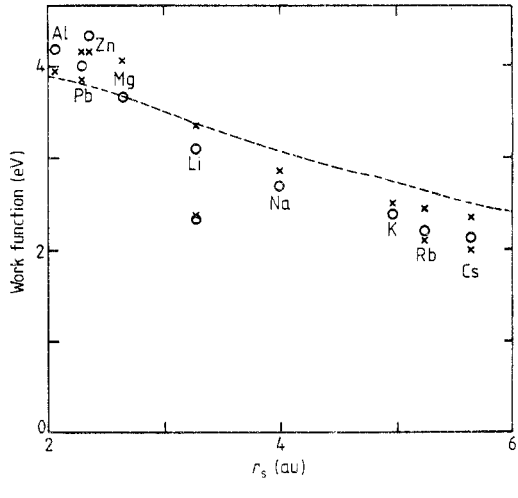

Figure 44. Work functions for simple metals. Broken curve: uniform positive background model; crosses: corrected with pseudopotential; circles: experimental results for polycrystalline materials (Lang and Kohn 1971).

work function increases only slowly with increasing electron density due to cancellation between changes in D and $\bar{\mu}$.

The effects of the ionic pseudopotential may be included in Lang and Kohn's results by first-order perturbation theory. To do this properly is a subtle problem, as there are first-order changes not only in the mean potential in the solid, hence $\bar{\mu}$, but also in the surface charge distribution and D. Lang and Kohn (1971) avoid this difficulty by using the fact that φ is the *energy change* when an electron is removed to infinity, and the effects of the pseudopotential on the energy can be found by standard first-order perturbation theory:

$$\delta\varphi = \int \mathrm{d}\boldsymbol{r}\, \delta V(\boldsymbol{r})[\rho_{N-1}(\boldsymbol{r}) - \rho_N(\boldsymbol{r})] \tag{4.3}$$

where δV is the change in potential due to the pseudopotential, ρ_N is the charge density with N electrons inside the solid and ρ_{N-1} is the charge density when one electron is removed to infinity. ρ_{N-1} can be found by a separate self-consistent calculation, in which there is a finite electric field outside the solid and zero field inside, and the resulting charge density difference $(\rho_{N-1} - \rho_N)$ is localised near the surface. The corrected work functions, averaged over different surfaces to compare with polycrystalline results, are shown in figure 44 and we see that the agreement with experiment is excellent.

5. Surface energy

Positive energy is needed to create a surface, because each atom has fewer neighbours with which to interact. However, it is not an easy quantity to calculate, because of the difficulty of separating surface and bulk energy in the energy expression (2.3), and cancellation between terms. In the case of semiconductors where there is a close connection between the first-principles description of the electronic structure and chemical bonding (§ 3.3), we should be able to estimate the surface energy from the number of broken bonds. As the cohesive energies of Ge and Si are 3.85 eV/atom and 4.63 eV/atom, respectively (Kittel 1976), we would expect (111) surface energies of about 3.85/4 eV and 4.63/4 eV per surface atom—2200 erg cm^{-2} for Ge and 2900 erg cm^{-2} for Si, about twice as large as the measured surface energy (Meyer and Sparnaay 1975). Chadi (1978) has estimated that the (2×1) reconstruction of Si (111) (§§ 3.3.3 and 6.3) lowers the energy by 0.36 eV/atom, reducing the surface energy to 2000 erg cm^{-2}. There is still a discrepancy between this and the reported value of 1200 erg cm^{-2}, showing that the local bonding picture is not particularly accurate.

The surface energy can also be estimated for transition metals, in which the main contribution to the bulk cohesive energy comes from the broadening of the atomic d levels into bands (§ 3.2) (Gelatt *et al* 1977). At the surface the d bands are narrowed, and if we approximate the density of states by a rectangle, its width w and height y must satisfy

$$wy = 5 \tag{5.1}$$

to conserve the number of states, and the second moment (3.2) is given by

$$w^3 y/12 = nh^2. \tag{5.2}$$

The one-electron energy (i.e. the first term in (2.3)) is given by $2y\int_{-w/2}^{E_F} E\,\mathrm{d}E$, so with

Z electrons the energy per atom is given by

$$E = (3/500)^{1/2} h \sqrt{n} (Z^2 - 10Z). \tag{5.3}$$

The one-electron contribution to the surface energy is the difference between (5.3) for surface and bulk atoms, giving:

$$\delta E = (3/500)^{1/2} h (Z^2 - 10Z)(\sqrt{n_b} - \sqrt{n_s}) \qquad \text{(per atom)} \tag{5.4}$$

where n_b is the number of bulk neighbours and n_s is the number of neighbours at the surface. The parabolic dependence of δE on the filling of the d bands is in qualitative agreement with experiment, as is its variation with n_s from surface to surface (Cyrot-Lackmann 1969): a tendency for the surface energy to be greatest when n_s is least (Maiya and Blakely 1967, Grenga and Kumar 1976). The absolute values of the surface energy given by the change in one-electron energy are too large, however (Cyrot-Lackmann 1969).

Reliable calculations of surface energy are based on evaluating (2.3) from a self-consistent calculation of the electronic structure. This has been carried out for the simple metals, in the jellium calculations of Lang and Kohn (1970), a variational calculation by Monnier and Perdew (1978) and the density matrix approach of Bohnen and Ying (1980). Appelbaum and Hamann (1978) obtained a good value for the surface energy of Cu (111) in a self-consistent slab calculation using an LCAO basis set (§ 2.3.3).

5.1. Surface energy of simple metals

It is convenient to rewrite the total energy of the electron–ion system (i.e. (2.3)+ the ion–ion electrostatic interaction) in terms of the electron kinetic energy T, the electron exchange-correlation energy E_{xc} and the total electrostatic energy E_{es} (Kohn and Sham 1965):

$$E = T + E_{xc} + E_{es}$$

with

$$\begin{aligned} T &= 2 \sum_{\substack{\text{occupied} \\ i}} \epsilon_i - \int \mathrm{d}\boldsymbol{r}\, V(\boldsymbol{r}) \rho_0(\boldsymbol{r}) \\ E_{es} &= \sum_I \int \mathrm{d}\boldsymbol{r}\, v_{ion}(\boldsymbol{r} - \boldsymbol{r}_I) \rho_0(\boldsymbol{r}) + \tfrac{1}{2} \int \mathrm{d}\boldsymbol{r}\, V_H(\boldsymbol{r}) \rho_0(\boldsymbol{r}) + E_{ion\text{-}ion}. \end{aligned} \tag{5.5}$$

The contributions of these terms to the surface energy of jellium, in which the positive ions are smeared out into the uniform positive background, are shown in table 2

Table 2. Jellium surface energies (Lang and Kohn 1970). Energies are in erg cm^{-2}.

r_s (au)	δT	δE_{es}	δE_{xc}	δE
2 (Al)	−5600	1330	3260	−1010
3	−720	170	750	200
4 (Na)	−145	40	265	160
5 (K)	−30	15	115	100
6	−5	10	55	60

(Lang and Kohn 1970). We see that the change in kinetic energy is negative, because the electrons lower their kinetic energy by spilling out of the surface (figure 10). This change in charge density increases the electrostatic energy, however—outside the solid the Hartree potential of the electrons is no longer cancelled by the potential of the positive background. The change in exchange-correlation energy, calculated in the local density approximation (2.6), also makes a very large positive contribution to δE. Altogether there is considerable cancellation between terms, and the net result is a positive surface energy at large r_s, in good agreement with experimental results for the alkalis (figure 45), but negative at small r_s. This reflects the instability of jellium at small r_s, which wants to increase its volume.

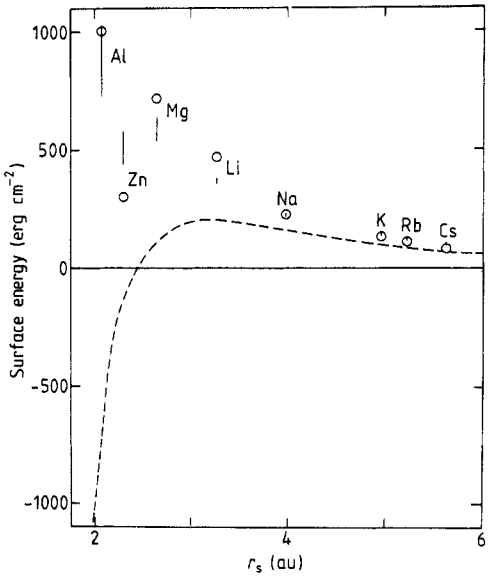

Figure 45. Surface energies of simple metals. Broken curve: uniform positive background model; bars: corrected with pseudopotential; circles: experimental results taken from extrapolation to $T = 0$ K of liquid surface tensions (Lang and Kohn 1970).

To obtain the correct behaviour at small r_s the ionic pseudopotential must be included—this can be done quite easily using first-order perturbation theory. When this is included the calculated surface energies are in very good agreement with experiment (figure 45), even at small r_s where the effects of the pseudopotential are important.

5.2. Surface exchange-correlation energy

Calculations of the surface energy depend to a large extent on the local density approximation (§ 2.1), and it is important to know whether this deals realistically with the electron–electron interactions in an inhomogeneous system like a metal with a surface. Thus the change in zero-point energy of the collective oscillations of the electrons—the plasmons—contributes to δE_{xc}, and because these involve long-range charge fluctuations it is not immediately clear whether this is an additional contribution to the local density approximation, or is somehow implicitly included.

The exchange-correlation energy can be found from the dielectric response function F, which gives the charge induced by an external charge $\delta\rho_{\text{ext}}$ with frequency ω (Hubbard 1958, Wikborg and Inglesfield 1975, 1977):

$$\delta\rho_{\text{ind}}(\boldsymbol{r}) = \int \mathrm{d}\boldsymbol{r}'\, F(\boldsymbol{r}, \boldsymbol{r}'; \omega)\delta\rho_{\text{ext}}(\boldsymbol{r}'). \tag{5.6}$$

From time-dependent perturbation theory F can be written in terms of the full many-body states of the system as

$$F(\boldsymbol{r}, \boldsymbol{r}'; \omega + \mathrm{i}\epsilon) = \sum_{f \neq 0} \langle 0|\hat{\rho}(\boldsymbol{r})|f\rangle\langle f|\hat{v}(\boldsymbol{r}')|0\rangle \left(\frac{1}{E_0 - E_f - (\omega + \mathrm{i}\epsilon)} + \frac{1}{E_0 - E_{\text{F}} + (\omega + \mathrm{i}\epsilon)} \right) \tag{5.7}$$

where $\hat{\rho}$ is the electron density operator, and $\hat{v}$ is the Coulomb interaction between the electrons and an external charge. So, integrating over positive frequencies, and using completeness we obtain

$$\int_0^\infty \mathrm{d}\omega\ \mathrm{Im}\, F(\boldsymbol{r}, \boldsymbol{r}'; \omega + \mathrm{i}\epsilon) = -\pi[\langle 0|\hat{\rho}(\boldsymbol{r})\hat{v}(\boldsymbol{r}')|0\rangle - \langle 0|\hat{\rho}(\boldsymbol{r})|0\rangle\langle 0|\hat{v}(\boldsymbol{r}')|0\rangle]. \tag{5.8}$$

But the expectation value of the interaction energy between electrons is given by

$$E_{\text{int}} = \tfrac{1}{2} \int \mathrm{d}\boldsymbol{r}\, \langle 0|\hat{\rho}(\boldsymbol{r})\hat{v}(\boldsymbol{r})|0\rangle + \text{constant} \tag{5.9}$$

so the change in interaction energy when a surface is made is

$$\delta E_{\text{int}} = -\frac{1}{2\pi} \int_0^\infty \mathrm{d}\omega \int \mathrm{d}\boldsymbol{r}\ \mathrm{Im}\, \delta F(\boldsymbol{r}, \boldsymbol{r}; \omega + \mathrm{i}\epsilon) + \tfrac{1}{2} \int \mathrm{d}\boldsymbol{r}\, \delta[V_{\text{H}}(\boldsymbol{r})\rho_0(\boldsymbol{r})] \tag{5.10}$$

the first term coming from exchange-correlation effects and the second term being the Hartree energy. The total exchange-correlation energy includes the change in kinetic energy due to switching on the electron–electron interaction, as well as the potential energy given by (5.10), but this can be obtained by integrating over the electron interaction strength parameter, giving:

$$\delta E_{\text{xc}} = -\int_0^1 \frac{\mathrm{d}(e^2)}{e^2} \int_0^\infty \frac{\mathrm{d}\omega}{2\pi} \int \mathrm{d}\boldsymbol{r}\ \mathrm{Im}\, \delta F(\boldsymbol{r}, \boldsymbol{r}; \omega + \mathrm{i}\epsilon). \tag{5.11}$$

This can be evaluated using the random phase approximation, equivalent to the time-dependent Hartree approximation in which the induced charge in (5.6) is given in terms of the *non-interacting* response function Λ by

$$\delta\rho_{\text{ind}}(\boldsymbol{r}) = \int \mathrm{d}\boldsymbol{r}'\Lambda(\boldsymbol{r}, \boldsymbol{r}'; \omega)[\delta\rho_{\text{ind}}(\boldsymbol{r}') + \delta\rho_{\text{ext}}(\boldsymbol{r}')]. \tag{5.12}$$

F is related to Λ by

$$F(\boldsymbol{r}, \boldsymbol{r}') = \Lambda(\boldsymbol{r}, \boldsymbol{r}') + \int \mathrm{d}\boldsymbol{r}''\Lambda(\boldsymbol{r}, \boldsymbol{r}'')F(\boldsymbol{r}'', \boldsymbol{r}') \tag{5.13}$$

and as Λ is proportional to e^2 it can be shown by integral equation theory that

$$\mathrm{Tr}\, F \equiv \int \mathrm{d}\boldsymbol{r}\, F(\boldsymbol{r}, \boldsymbol{r}) = -e^2 \frac{\partial}{\partial(e^2)} \ln \det(1 - \Lambda). \tag{5.14}$$

Substituting this into (5.11) we finally obtain our expression for the change in exchange-correlation energy:

$$\delta E_{xc} = \int_0^\infty \frac{d\omega}{2\pi} \operatorname{Im} \delta[\ln \det (1 - \Lambda)]. \tag{5.15}$$

Λ can be found explicitly for certain simple models, and Wikborg and Inglesfield (1975, 1977) used (5.15) to calculate δE_{xc} for the infinite barrier model of a metal surface, in which the electrons are confined by an infinite potential step at $z = 0$. To show where the contributions to δE_{xc} come from it is convenient to carry out a wavevector decomposition of (5.15):

$$\delta E_{xc} = \int \frac{d^2\boldsymbol{K}}{4\pi^2} \int_0^\infty \frac{d\omega}{2\pi} \delta\epsilon_{xc}(\boldsymbol{K}, \omega) \tag{5.16}$$

and figure 46 shows $\delta\epsilon_{xc}$ as a function of ω at $\boldsymbol{K} = 0.3$ au for the electron density of Al. We see that there are steps of about π at $\omega = 0.51$ au, the surface plasmon frequency at this wavevector, and of about $-\pi/2$ at $\omega = 0.62$ au, the frequency of the bulk plasmon with wavevector $\boldsymbol{k} = (\boldsymbol{K}, 0)$. These give contributions to δE_{xc} of $\omega_s/2$,

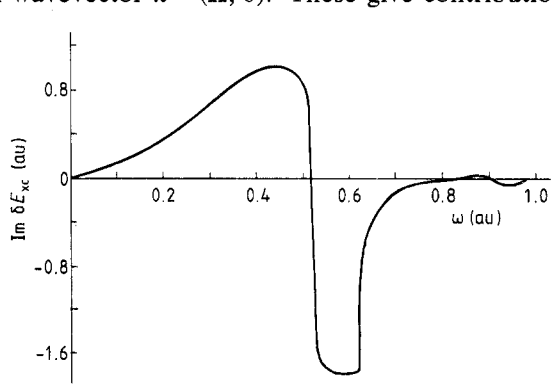

Figure 46. Contribution to surface exchange-correlation energy $\delta\epsilon_{xc}$ at $K = 0.3$ au as a function of ω, at electron density corresponding to Al (Wikborg and Inglesfield 1975).

the surface plasmon zero-point energy, and about $-\omega_b/4$, the zero-point energy of half a bulk plasmon removed on making the surface. However, when we carry out the integration in (5.16) we obtain the results given in table 3, in excellent agreement with δE_{xc} found using the local density approximation for the infinite barrier charge density profile (Lang and Sham 1975, Langreth and Perdew 1977). Even though the change in plasmon zero-point energy enters the contribution to δE_{xc} at each wavevector, the exchange-correlation energy comes from the *spatially averaged* interaction

Table 3. Surface exchange-correlation energies in the infinite barrier model. The results from the full calculation were obtained by Wikborg and Inglesfield (1975, 1977), and using the local density approximation by Lang and Sham (1975) and Langreth and Perdew (1977). Energies are in erg cm^{-2}.

r_s (au)	δE_{xc} (full calculation)	δE_{xc} (local density approximation)
2.07	1350	1241
4	190	184
6	60	58

of an electron with the surrounding electron distribution, and this is reproduced to *better than 10% by the local density approximation.*

The success of the local density approximation means that it is usually unnecessary to go beyond it—a fortunate situation, as the corrections are generally difficult to evaluate. The local density expression (2.6) is the first term in a functional expansion of E_{xc}, and subsequent terms involve the density gradient (Geldart and Rasolt 1976). However, the use of the first gradient correction actually worsens the value of δE_{xc} with the density variations found at metal surfaces (Perdew *et al* 1977), and it is better to stay with the local density approximation. The most promising approach to finding the corrections to the local density approximation has come from the work of Langreth and Perdew (1977, 1980) who decompose δE_{xc} into three-dimensional wavevector contributions, rather than the two-dimensional decomposition we used above (5.16). The local density approximation works well at large k, and it is only at small k (corresponding to long-wavelength density fluctuations) that corrections need to be made. The exact behaviour as $k \to 0$ is dominated by the plasmon zero-point energy, and knowing this it is possible to estimate the corrections to the local density approximation.

6. Electronic structure and surface crystallography

The stable atomic geometry at a surface comes from minimising the total energy—an immediate consequence of this is that the equilibrium shape of a crystal depends on the variation of surface energy from surface to surface (§ 5) (Somorjai 1976). Here we are more concerned with the atomic structure of particular perfect surfaces, and the way that changes in electronic structure (§ 3) lead to changes in structure compared with the bulk, with surface relaxation and reconstruction.

6.1. Relaxation of metal surfaces

LEED experiments suggest that the top interlayer spacing tends to contract in metals, especially on open surfaces like FCC (110) and BCC (001) (Van Hove and Tong 1979). In the case of FCC Al the decrease in interlayer spacing is probably 10–15% on the (110) surface, with no contraction on the (001) surface (Van Hove and Tong 1979) and 2% expansion on the (111) surface (Jona *et al* 1980); the (001) surface of BCC W shows an 8% contraction (Marsh *et al* 1980). This behaviour is contrary to the prediction of pair force models, which nearly always give outward relaxations (Johnson and White 1976)—the energy of metals cannot generally be written in terms of pair potentials, except for the structure-dependent part of the energy of bulk s–p bonded metals (Heine and Weaire 1970).

The tendency for surface contraction has been explained by Finnis and Heine (1974) using the Hellman–Feynman theorem, which says that the force on an ion is just the electrostatic force from the other ions and the self-consistent electron density $\rho_0(\boldsymbol{r})$. If the surface atomic cells were undistorted (figure 42), each ion would be at the centre of its own Wigner–Seitz cell, feeling no net electric field from the charge in this cell, nor from the other cells because they are nearly spherical: there would be no surface relaxation. However, we know that the surface charge tends to be smoothed (§ 4), and the redistribution of charge produces a force on the surface ions in their ideal positions. If we assume that the surface charge is cut off on a plane

surface, corresponding to complete smoothing, it is straightforward to find the electrostatic centre of gravity for the distorted surface cells, at which an ion experiences no net field: this corresponds to contractions of 1.6% for FCC (111), 4.6% for FCC (001) and 16% for FCC (110), giving at least the right trends. Landman *et al* (1980) have used various one-dimensional models of the surface charge density, including the Lang–Kohn self-consistent jellium results (§ 3.1) to calculate the forces on the ions, and obtain similar results to Finnis and Heine, apart from a small expansion (~1%) on Al (111).

The lattice relaxations of Al have been studied in more detail by Perdew and Monnier (1980), using a variational method in which a trial wavefunction satisfying a one-dimensional Schrödinger equation is inserted into the full three-dimensional Hamiltonian. They vary the position of the first atomic plane and find that the total energy is minimised with a 1% expansion on (111), a 7% contraction on (001) and a contraction greater than 10% on (110).

Charge density smoothing is greatest in s–p bonded metals, like Al (figure 12), where all the valence electrons are nearly free. In the transition and noble metals the charge distribution of the tightly-bound d electrons is not smoothed in the same way (figures 21 and 29), and we cannot use the argument of Finnis and Heine (1974) to describe their contribution to surface relaxation (though the Hellman–Feynman theorem can still be used, of course, if we know $\rho_0(\boldsymbol{r})$ accurately enough). The band narrowing in the (001) surface density of states of Mo and W (§ 3.2.1 and figure 20) seems to be responsible for the contractions of 10% (Clarke 1980) and 8% (Marsh *et al* 1980) found, respectively, at these surfaces. A tight-binding calculation for Mo (001) shows that the increased interaction of the surface atoms with the substrate on the contracted surface transfers weight to the wings of the d-band density of states (Desjonquères 1979), and because the d band is half full this leads to a reduction in energy. Figure 47 gives the surface density of states for the ideal and relaxed (12% contracted) Mo (001) surface, found using the matching Green function method (Inglesfield 1978c): this also shows an increase in weight in the 'bonding' region of the density of states ($E \lesssim 0.25$ au) together with a downward shift in the central peak.

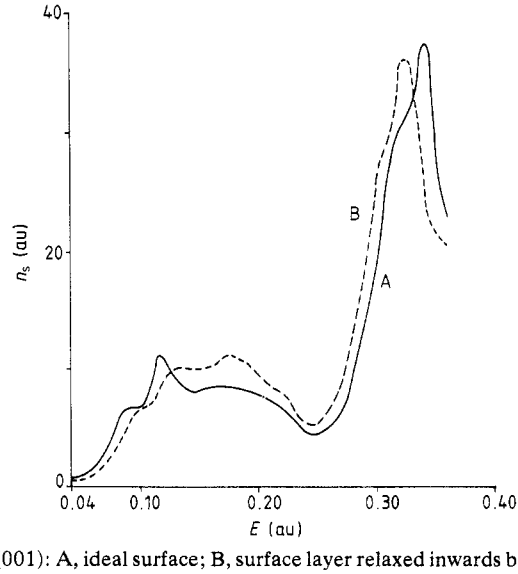

Figure 47. $n_s(E)$ for Mo (001): A, ideal surface; B, surface layer relaxed inwards by 12% (Inglesfield 1978c).

Both of these effects lower the one-electron energy, though the shift in the peak will have to be compensated for by changes in the surface potential in a self-consistent calculation. The surface contraction on the BCC (001) surface is thus due to the large change in electronic structure on this open surface. It is interesting that W, showing a smaller surface contraction than Mo, has the greater bulk modulus—in other words, the forces resisting contraction are greater in W than Mo.

6.2. Mo and W (001) surface reconstructions

At about room temperature W (001) goes from the (1×1) structure (relaxed but not reconstructed) to the low-temperature $(\sqrt{2}\times\sqrt{2})$ R45° structure (figure 2(*a*)) in an apparently continuous and reversible phase transition (Debe and King 1979); the Mo (001) surface undergoes a similar phase transition, though the wavevector of reconstruction is $0.9(\pi/a, \pi/a)$ rather than $(\pi/a, \pi/a)$ (Felter *et al* 1977). The incommensurability of the Mo (001) reconstruction is reminiscent of transition-metal dichalcogenide layer compounds like $TaSe_2$, essentially two-dimensional materials which show phase transitions from an ideal high-temperature phase to an incommensurate phase (Moncton *et al* 1977). In some of these cases a Fermi surface instability plays a role (Tosatti 1975): the two-dimensional Fermi surface has flattened regions, and it becomes energetically favourable for a reconstruction to occur with the (incommensurate) wavevector which spans the Fermi surface, so that an energy gap opens up over the flattened regions. This is sometimes called a charge density wave (CDW) instability (Chan and Heine 1973), because the flattened regions of Fermi surface lead to screening anomalies, with screening charge tending to pile up with the spanning wavevector. Calculations for Mo and W (001) predicted a flat line of surface states at E_F in the surface Brillouin zone (Inglesfield 1978c, Krakauer *et al* 1979b), and it was thus suggested that the surface phase transitions were due to an analogous CDW instability (Inglesfield 1978c, Tosatti 1978). However, as we have seen in § 3.2.2, angle-resolved photoemission experiments show a very curved surface-state Fermi line (Campuzano *et al* 1981), and we must now reject this theory of the phase transitions (Inglesfield 1981).

Rather than surface states at a particular point in the surface Brillouin zone driving the transition, more general features of $n_s(E)$ are probably responsible for the Mo and W (001) surface reconstructions. Indeed, on general grounds we would expect some sort of instability because E_F is close to the central peak in the surface density of states (figure 20): any atomic displacements which broaden or split the peak will lower the energy. When the Mo (001) surface is reconstructed to a $(\sqrt{2}\times\sqrt{2})$ R45° structure (with $\boldsymbol{Q} = (\pi/a, \pi/a)$ rather than the observed $0.9(\pi/a, \pi/a)$ for simplicity of calculation) there are several energetically favourable changes in the surface density of states (figure 48) (Inglesfield 1978c). We see an increase in $n_s(E)$ at low energies, weight mainly being transferred to the $m = 1$ d_{zx} and d_{zy} orbitals associated with bulk bonding (§ 3.2.1), and a downward shift in the average energy of the central peak: these changes are very similar to what we found in surface relaxation, and are due to an increased interaction of the surface atoms with their neighbours in the surface and substrate. This calculation also shows a kink developing in n_s at E_F due to the surface-state coupling—this only gives a small contribution to the energy (Inglesfield 1979b), and is in any case overestimated in this calculation with the spurious straight line of surface states at $\boldsymbol{K} = (\pi/2a, \pi/2a)$. An important contribution to the energy change in a tight-binding calculation is a broadening of the central peak on reconstruction (Terakura *et al* 1981).

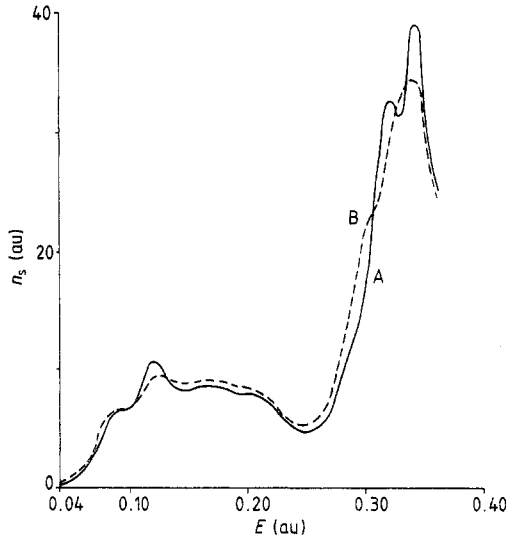

Figure 48. $n_s(E)$ for Mo (001): A, ideal surface; B, $(\sqrt{2}\times\sqrt{2})$ R45° reconstructed surface with $\boldsymbol{Q} = (\pi/a, \pi/a)$ (figure 2(*a*)) (Inglesfield 1978c).

The tendency of the surface atoms to increase their interactions with one another, and the substrate, due to the peak in $n_s(E)$ (itself a consequence of the open (001) BCC surface) leads to other instabilities of the W and Mo (001) surfaces under different conditions. The adsorption of even a small amount of H causes a reconstruction with displacements in the ⟨10⟩ directions (King and Thomas 1980), as the H atoms go into bridge sites and enhance this particular instability. These displacements have been studied by following the core shifts (van der Veen *et al* 1981): the clean W (001) surface shows a lineshape which can be decomposed into two core shifts, one component having a core shift of 0.35 eV to less binding energy compared with the bulk, and the other a shift of 0.13 eV. These presumably come from surface atoms in unreconstructed and reconstructed domains, the displaced atoms having much smaller core shifts as their interaction with neighbours is greater, as in the bulk. (The presence of domains is probably due to surface defects inhibiting the phase transition (Debe and King 1979).) When H is adsorbed the fraction of displaced atoms increases, till by 0.2 coverage all the surface atoms are displaced and show the smaller core shift. Another instability is produced by adsorption of N on W (001), and at 0.4 fractional coverage an island structure occurs in which each N atom, occupying a four-fold coordinated site, pulls the surrounding W atoms towards itself (Griffiths *et al* 1981).

6.3. Semiconductor surface reconstructions

The reconstructions on semiconductor surfaces which we discussed in § 3.3 are driven by the dangling bonds: in the (2×1) reconstructions, doubling the surface unit cell lowers the energy of the occupied dangling bonds (figures 33 and 36), and this stabilises the reconstructions (Appelbaum and Hamann 1975, Chadi 1978, 1979a, b). To find the actual atomic displacements, the total energy given by (2.3)+ the ion–ion electrostatic energy must be minimised, and Chadi (1978, 1979b) rewrites this as

$$E = 2 \sum_{\substack{\text{occupied} \\ i}} \epsilon_i + U \tag{6.1}$$

where

$$U = E_{\text{ion-ion}} - \tfrac{1}{2}\int \mathrm{d}\boldsymbol{r} \int \mathrm{d}\boldsymbol{r}'\, \rho_0(\boldsymbol{r}) v(\boldsymbol{r}-\boldsymbol{r}')\rho_0(\boldsymbol{r}') - \left(\int \mathrm{d}\boldsymbol{r}\, V_{\text{xc}}(\boldsymbol{r})\rho_0(\boldsymbol{r}) - E_{\text{xc}}\right). \quad (6.2)$$

U is certainly short-ranged, as the first and second terms in (6.2) tend to cancel beyond the screening length, and the exchange-correlation energy depends on local densities. This term is expanded in terms of atomic displacements, whose coefficients are assumed to be transferable from the bulk where they are fitted so that (6.1) gives the correct equilibrium volume and elastic constants. The first term in (6.1), the *band structure energy*, can easily be found from calculations of the electronic structure—Chadi (1978, 1979b) uses a tight-binding method with fitted parameters. The reduction in energy by dimerisation of the dangling bonds, and back bond formation, is contained in the band structure term, and this tends to be opposed by strain effects contained in U. Using this method, atomic displacements have been obtained for the (2×1) reconstructions of Si (111) and (001), and relaxations of GaAs and ZnSe (110) (Chadi 1978, 1979a, b) which are generally in very good agreement with experiment.

By analogy with the (2×1) reconstruction of Si (111) we can understand the local buckling suggested for the (7×7) reconstruction (figure 33) (§ 3.3, Chadi *et al* 1980, McRae and Caldwell 1981); the question remains—why should the (7×7) structure be superimposed on the local buckling? Tosatti and Anderson (1974) suggested that the new surface Brillouin zone boundaries introduced by the (7×7) reconstruction would nicely enclose the dangling bond Fermi line, and this would make the energy gap at the zone boundaries especially effective in lowering the energy of the occupied surface states. This might still have a marginal effect even when the local buckling itself lowers the energy of the states, but it really seems inappropriate to consider the shape of the Fermi line of the ideal surface when the reconstruction probably involves quite large displacements. What seems conclusive evidence against the influence of the Fermi line is the stability of the (7×7) geometry to hydrogenation, which removes both the dangling bond surface states and the buckling (McRae and Caldwell 1981). A possible answer is that the change in electronic structure in the top layer of atoms means that they have a different effective lattice constant from the substrate, and misfit strain energy determines the optimum size and separation of islands of excess atoms on the surface (Phillips 1980).

Acknowledgments

I thank G C Aers, T B Grimley, D A King and J B Pendry for many useful discussions. I am grateful to the various authors for permission to use their figures in this review.

References

Akoh H and Tasaki A 1978 *J. Appl. Phys.* **49** 1410–2
Alldredge G P and Kleinman L 1974 *Phys. Rev.* B **10** 559–73
Appelbaum J A, Baraff G A and Hamann D R 1975 *Phys. Rev.* B **11** 3822–31
Appelbaum J A and Hamann D R 1972 *Phys. Rev.* B **6** 2166–77
—— 1973 *Phys. Rev. Lett.* **31** 106–9
—— 1975 *Phys. Rev.* B **12** 1410–7
—— 1978 *Solid St. Commun.* **27** 881–3

Arlinghaus F J, Gay J G and Smith J R 1980 *Phys. Rev.* B **21** 2055–9
von Barth U and Hedin L 1972 *J. Phys. C: Solid St. Phys.* **5** 1629–42
Bohnen K P and Ying S C 1980 *Phys. Rev.* B **22** 1806–17
Brennan S, Stöhr J, Jaeger R and Rowe J E 1980 *Phys. Rev. Lett.* **45** 1414–8
Campuzano J C, Inglesfield J E, King D A and Somerton C 1981 *J. Phys. C: Solid St. Phys.* **14** 3099–113
Campuzano J C, King D A, Somerton C and Inglesfield J E 1980 *Phys. Rev. Lett.* **45** 1649–52
Cardillo M J 1981 *Phys. Rev.* B **23** 4279–82
Caruthers E, Kleinman L and Alldredge G P 1973 *Phys. Rev.* B **8** 4570–7
—— 1974 *Phys. Rev.* B **9** 3325–9
Chabal Y J, Rowe J E and Zwemer D A 1981 *Phys. Rev. Lett.* **46** 600–3
Chadi D J 1978 *Phys. Rev. Lett.* **41** 1062–5
—— 1979a *Phys. Rev. Lett.* **43** 43–7
—— 1979b *Phys. Rev.* B **19** 2074–82
Chadi D J, Bauer R S, Williams R H, Hansson G V, Bachrach R Z, Mikkelsen J C, Houzay F, Guichar G M, Pinchaux R and Petroff Y 1980 *Phys. Rev. Lett.* **44** 799–802
Chadi D J and Cohen M L 1975 *Phys. Rev.* B **11** 732–7
Chan S-K and Heine V 1973 *J. Phys. F: Metal Phys.* **3** 795–809
Chelikowsky J R and Cohen M L 1976 *Phys. Rev.* B **13** 826–34
—— 1979 *Solid St. Commun.* **29** 267–71
Chelikowsky J R, Schlüter M, Louie S G and Cohen M L 1975 *Solid St. Commun.* **17** 1103–6
Chiarotti G, Nannarone S, Pastore R and Chiaradia P 1971 *Phys. Rev.* B **4** 3398–402
Clarke L J 1980 *Surf. Sci.* **91** 131–52
Cohen M L and Heine V 1970 *Solid St. Phys.* **24** 37–248
Cyrot-Lackmann F 1969 *Surf. Sci.* **15** 535–48
Debe M K and King D A 1979 *Surf. Sci.* **81** 193–237
Denninger G, Dose V and Bonzel H P 1982 to be published
Desjonquères M C 1979 *J. Physique Lett.* **40** L249–52
Desjonquères M C and Cyrot-Lackmann F 1975 *J. Phys. F: Metal Phys.* **5** 1368–84
Dietz E and Eastman D E 1978 *Phys. Rev. Lett.* **41** 1674–7
Duc T M, Guillot C, Lassailly Y, Lecante J, Jugnet Y and Vedrine J C 1979 *Phys. Rev. Lett.* **43** 789–92
Eastman D E, Himpsel F J and Knapp J A 1980 *Phys. Rev. Lett.* **44** 95–8
Eberhardt W, Plummer E W, Horn K and Erskine J 1980 *Phys. Rev. Lett.* **45** 273–6
Edwards D M 1979 *Trends in Physics 1978* ed M M Woolfson (Bristol: Adam Hilger) pp 150–63
Feder R, Mönch W and Auer P P 1979 *J. Phys. C: Solid St. Phys.* **12** L179–84
Feder R and Sturm K 1975 *Phys. Rev.* B **12** 537–48
Feibelman P J, Appelbaum J A and Hamann D R 1979 *Phys. Rev.* B **20** 1433–43
Felter T E, Barker R A and Estrup P J 1977 *Phys. Rev. Lett.* **38** 1138–41
Feuerbacher B, Fitton B and Willis R F (ed) 1978 *Photoemission and the Electronic Properties of Surfaces* (New York: Wiley)
Finnis M V and Heine V 1974 *J. Phys. F: Metal Phys.* **4** L37–41
Forstmann F 1978 *Photoemission and the Electronic Properties of Surfaces* ed B Feuerbacher, B Fitton and R F Willis (New York: Wiley) pp 193–226
Friedel J 1973 *J. Phys. F: Metal Phys.* **3** 785–94
—— 1976 *J. Physique* **37** 883–94
García-Moliner F and Flores F 1976 *J. Phys. C: Solid St. Phys.* **9** 1609–34
Gartland P O, Berge S and Slagsvold B J 1972 *Phys. Rev. Lett.* **28** 738–9
Gartland P O and Slagsvold B J 1975 *Phys. Rev.* B **12** 4047–58
Gelatt C D, Ehrenreich H and Watson R E 1977 *Phys. Rev.* B **15** 1613–28
Geldart D J W and Rasolt M 1976 *Phys. Rev.* B **13** 1477–88
Grenga H E and Kumar R 1976 *Surf. Sci.* **61** 283–90
Grepstad J K, Gartland P O and Slagsvold B J 1976 *Surf. Sci.* **57** 348–62
Griffiths K, Kendon C, King D A and Pendry J B 1981 *Phys. Rev. Lett.* **46** 1584–7
Gudat W and Eastman D E 1976 *J. Vacuum Sci. Technol.* **13** 831–7
Gunnarsson O, Harris J and Jones R O 1977 *Phys. Rev.* B **15** 3027–38
Gurman S J and Pendry J B 1973 *Phys. Rev. Lett.* **31** 637–9
Haneman D 1961 *Phys. Rev.* **121** 1093–100
—— 1968 *Phys. Rev.* **170** 705–18
—— 1975 *Surface Physics of Semiconductors* ed C G Scott and C E Reed (New York: Academic) pp 1–94

Hansson G V, Bachrach R Z, Bauer R S, Chadi D J and Göpel W 1980 *Surf. Sci.* **99** 13–27
Hansson G V and Flodström S A 1978 *Phys. Rev.* B **18** 1562–71
—— 1979 *Phys. Rev.* B **19** 3329
Harrison W A 1976 *Surf. Sci.* **55** 1–19
Haydock R 1980 *Solid St. Phys.* **35** 215–94
Haydock R and Kelly M J 1973 *Surf. Sci.* **38** 139–48
Hedin L and Lundqvist S 1969 *Solid St. Phys.* **23** 1–181
Heimann P, Hermanson J, Miosga H and Neddermeyer H 1979 *Phys. Rev. Lett.* **42** 1782–4
Heine V 1963 *Proc. Phys. Soc.* **81** 300–10
—— 1980 *Solid St. Phys.* **35** 1–127
Heine V and Hodges C H 1972 *J. Phys. C: Solid St. Phys.* **5** 225–30
Heine V and Jones R O 1969 *J. Phys. C: Solid St. Phys.* **2** 719–32
Heine V and Weaire D 1970 *Solid St. Phys.* **24** 249–463
Higinbotham J and Haneman D 1973 *Surf. Sci.* **34** 450–6
Himpsel F J and Eastman D E 1979 *J. Vacuum Sci. Technol.* **16** 1297–9
Hochstrasser G and Antonini J F 1972 *Surf. Sci.* **32** 644–64
Hohenberg P and Kohn W 1964 *Phys. Rev.* **136** B864–71
Holmes M W and Gustafsson T 1981 *Phys. Rev. Lett.* **47** 443–6
Holmes M W and Inglesfield J E 1979 *Surf. Sci.* **89** 133–41
Hubbard J 1958 *Proc. R. Soc.* A **244** 199–211
Huijser A, van Laar J and van Rooy T L 1977 *Surf. Sci.* **62** 472–86
—— 1978 *Phys. Lett.* **65A** 337–9
Ibach H and Rowe J E 1974 *Surf. Sci.* **43** 481–92
Ihm J, Cohen M L and Chadi D J 1980 *Phys. Rev.* B **21** 4592–9
Inglesfield J E 1978a *Surf. Sci.* **76** 355–78
—— 1978b *Surf. Sci.* **76** 379–96
—— 1978c *J. Phys. C: Solid St. Phys.* **11** L69–72
—— 1979a *J. Phys. C: Solid St. Phys.* **12** L349–54
—— 1979b *J. Phys. C: Solid St. Phys.* **12** 149–65
—— 1981 *Vacuum* to be published
Inglesfield J E and Holland B W 1981 *The Chemical Physics of Solid Surfaces and Heterogeneous Catalysis* vol 1, ed D A King and D P Woodruff (Amsterdam: Elsevier) pp 355–63
Inglesfield J E and Wikborg E 1975 *J. Phys. F: Metal Phys.* **5** 1475–89
Jepsen O, Madsen J and Andersen O K 1978 *Phys. Rev.* B **18** 605–15
Johnson R A and White P J 1976 *Phys. Rev.* B **13** 5293–302
Jona F, Shih H D, Jepsen D W and Marcus P M 1979 *J. Phys. C: Solid St. Phys.* **12** L455–61
Jona F, Sondericker D and Marcus P M 1980 *J. Phys. C: Solid St. Phys.* **13** L155–8
Jones R O 1972 *J. Phys. C: Solid St. Phys.* **5** 1615–8
Kelly M J 1980 *Solid St. Phys.* **35** 295–383
Kerker G P, Ho K M and Cohen M L 1978 *Phys. Rev.* B **18** 5473–83
King D A and Thomas G 1980 *Surf. Sci.* **92** 201–36
Kittel C 1976 *Introduction to Solid State Physics* (New York: Wiley) 5th edn
Kleinman L 1975a *Phys. Rev.* B **11** 858–61
—— 1975b *Phys. Rev.* B **11** 3900–3
Knapp J A and Lapeyre G J 1976 *J. Vacuum Sci. Technol.* **13** 757–60
Koelling D D 1981 *Rep. Prog. Phys.* **44** 139–212
Kohn W and Sham L J 1965 *Phys. Rev.* **140** A1133–8
Krakauer H, Posternak M and Freeman A J 1978 *Phys. Rev. Lett.* **41** 1072–5
—— 1979a *Phys. Rev.* B **19** 1706–19
—— 1979b *Phys. Rev. Lett.* **43** 1885–9
Krakauer H, Posternak M, Freeman A J and Koelling D D 1981 *Phys. Rev.* B **23** 3859–76
Krane K J and Raether H 1976 *Phys. Rev. Lett.* **37** 1355–7
Lander J J and Morrison J 1963 *J. Appl. Phys.* **34** 1411–5
Landman U, Hill R N and Mostoller M 1980 *Phys. Rev.* B **21** 448–57
Lang N D 1973 *Solid St. Phys.* **28** 225–300
Lang N D and Kohn W 1970 *Phys. Rev.* B **1** 4555–68
—— 1971 *Phys. Rev.* B **3** 1215–23
Lang N D and Sham L J 1975 *Solid St. Commun.* **17** 581–4

Langreth D C and Perdew J P 1977 *Phys. Rev.* B **15** 2884–901
—— 1980 *Phys. Rev.* B **21** 5469–93
Larsson C G and Nilsson P O 1981 *Phys. Lett.* **85A** 393–4
Levine J D and Mark P 1966 *Phys. Rev.* **144** 751–63
Ley L, Kerker G P and Mårtensson N 1981 *Phys. Rev.* B **23** 2710–7
Liebermann L, Clinton J, Edwards D M and Mathon J 1970 *Phys. Rev. Lett.* **25** 232–5
Louie S G, Ho K-M, Chelikowsky J R and Cohen M L 1977 *Phys. Rev.* B **15** 5627–35
McCaffrey J W, Anderson J R and Papaconstantopoulos D A 1973 *Phys. Rev.* B **7** 674–84
McRae E G and Caldwell C W 1981 *Phys. Rev. Lett.* **46** 1632–5
Maiya P S and Blakely J M 1967 *J. Appl. Phys.* **38** 698–704
Many A, Goldstein Y and Grover N B 1971 *Semiconductor Surfaces* (Amsterdam: North-Holland)
Marsh F S, Debe M K and King D A 1980 *J. Phys. C: Solid St. Phys.* **13** 2799–805
Marsh J B and Farnsworth H E 1964 *Surf. Sci.* **1** 3–21
Meyer F and Sparnaay M J 1975 *Surface Physics of Phosphors and Semiconductors* ed C G Scott and C E Reed (New York: Academic) pp 321–410
Miller D J and Haneman D 1979 *J. Vacuum Sci. Technol.* **16** 1270–85
Mönch W 1979 *Surf. Sci.* **86** 672–99
Moncton D E, Axe J D and DiSalvo F J 1977 *Phys. Rev.* B **16** 801–19
Monnier R and Perdew J P 1978 *Phys. Rev.* B **17** 2595–611
Moore I D and Pendry J B 1978 *J. Phys. C: Solid St. Phys.* **11** 4615–22
Moruzzi V L, Janak J F and Williams A R 1978 *Calculated Electronic Properties of Metals* (Oxford: Pergamon)
Nicolaou N and Modinos A 1975 *Phys. Rev.* B **11** 3687–96
Nieminen R M and Hodges C H 1976 *J. Phys. F: Metal Phys.* **6** 573–85
Nyberg C 1977 *Surf. Sci.* **65** 389–98
Park R L 1979 *Surf. Sci.* **86** 504–15
Park R L and Houston J E 1972 *Phys. Rev.* B **6** 1073–81
Parke A W, McKinley A, Williams R H and Srivastava G P 1980 *J. Phys. C: Solid St. Phys.* **13** L369–74
Pendry J B 1974 *Low Energy Electron Diffraction* (New York: Academic)
—— 1980a *J. Phys. C: Solid St. Phys.* **13** 1159–74
—— 1980b *Phys. Rev. Lett.* **45** 1356–8
Pendry J B and Gurman S J 1975 *Surf. Sci.* **49** 87–105
Pendry J B and Hopkinson J F L 1978a *J. Phys. F: Metal Phys.* **8** 1009–17
—— 1978b *J. Physique* C **4** 142–8
Perdew J P, Langreth D C and Sahni V 1977 *Phys. Rev. Lett.* **38** 1030–3
Perdew J P and Monnier R 1980 *J. Phys. F: Metal Phys.* **10** L287–91
Pettifor D G 1970 *J. Phys. C: Solid St. Phys.* **3** 367–77
Phillips J C 1968 *Phys. Rev.* **166** 832–8
—— 1980 *Phys. Rev. Lett.* **45** 905–8
Plummer E W and Eberhardt W 1979 *Phys. Rev.* B **20** 1444–53
Plummer E W and Gadzuk J W 1970 *Phys. Rev. Lett.* **25** 1493–5
Posternak M, Krakauer H, Freeman A J and Koelling D D 1980 *Phys. Rev.* B **21** 5601–12
Ritchie R H 1972 *Phys. Lett.* **38A** 189–90
Rivière J C 1969 *Solid St. Surf. Sci.* **1** 179–289
Rowe J E, Ibach H and Froitzheim H 1975 *Surf. Sci.* **48** 44–58
Schlüter M, Chelikowsky J R, Louie S G and Cohen M L 1975 *Phys. Rev.* B **12** 4200–14
Seitz F 1940 *The Modern Theory of Solids* (New York: McGraw-Hill)
Shockley W 1939 *Phys. Rev.* **56** 317–23
Smith J R, Gay J G and Arlinghaus F J 1980 *Phys. Rev.* B **21** 2201–21
Smoluchowski R 1941 *Phys. Rev.* **60** 661–74
Somorjai G A 1976 *Treatise on Solid State Chemistry* vol 6A, ed N B Hannay (New York: Plenum) pp 1–55
Spanjaard D, Jepsen D W and Marcus P M 1979 *Phys. Rev.* B **19** 642–54
Strayer R W, Mackie W and Swanson L W 1973 *Surf. Sci.* **34** 225–48
Terakura I, Terakura K and Hamada N 1981 *Surf. Sci.* **103** 103–17
Thiry P, Chandesris D, Lecante J, Guillot C, Pinchaux R and Petroff Y 1979 *Phys. Rev. Lett.* **43** 82–5
Tong S Y, Lubinsky A R, Mrstik B J and van Hove M A 1978 *Phys. Rev.* B **17** 3303–9
Tosatti E 1975 *Festkörperprobleme* vol XV (Braunschweig: Vieweg) pp 113–47
—— 1978 *Solid St. Commun.* **25** 637–40

Tosatti E and Anderson P W 1974 *Solid St. Commun.* **14** 773–7
Treglia G, Desjonquères M C, Ducastelle F and Spanjaard D 1980 *Solid St. Phys.* **13** 6063–72
Van Hove M A and Tong S Y 1979 *Surface Crystallography by LEED* (Berlin: Springer-Verlag)
van der Veen J F, Himpsel F J and Eastman D E 1981 *Solid St. Commun.* **40** 57–60
Waclawski B J and Plummer E W 1972 *Phys. Rev. Lett.* **29** 783–6
Wang C S and Callaway J 1977 *Phys. Rev.* B **15** 298–306
Wang C S and Freeman A J 1979 *Phys. Rev.* B **19** 793–805
—— 1980 *Phys. Rev.* B **21** 4585–91
Wang C S, Freeman A J, Krakauer H and Posternak M 1981 *Phys. Rev.* B **23** 1685–90
Weng S-L, Plummer E W and Gustafsson T 1978 *Phys. Rev.* B **18** 1718–40
Werner C, Schulte F K and Bross H 1975 *J. Phys. C: Solid St. Phys.* **8** 3817–24
Wikborg E and Inglesfield J E 1975 *Solid St. Commun.* **16** 335–9
—— 1977 *Phys. Scr.* **15** 37–55
Yndurain F and Elices M 1972 *Surf. Sci.* **29** 540–54
Ziman J M 1972 *Principles of the Theory of Solids* (Cambridge: Cambridge University Press)
Zunger A, Kerker G P and Cohen M L 1979 *Phys. Rev.* B **20** 581–93